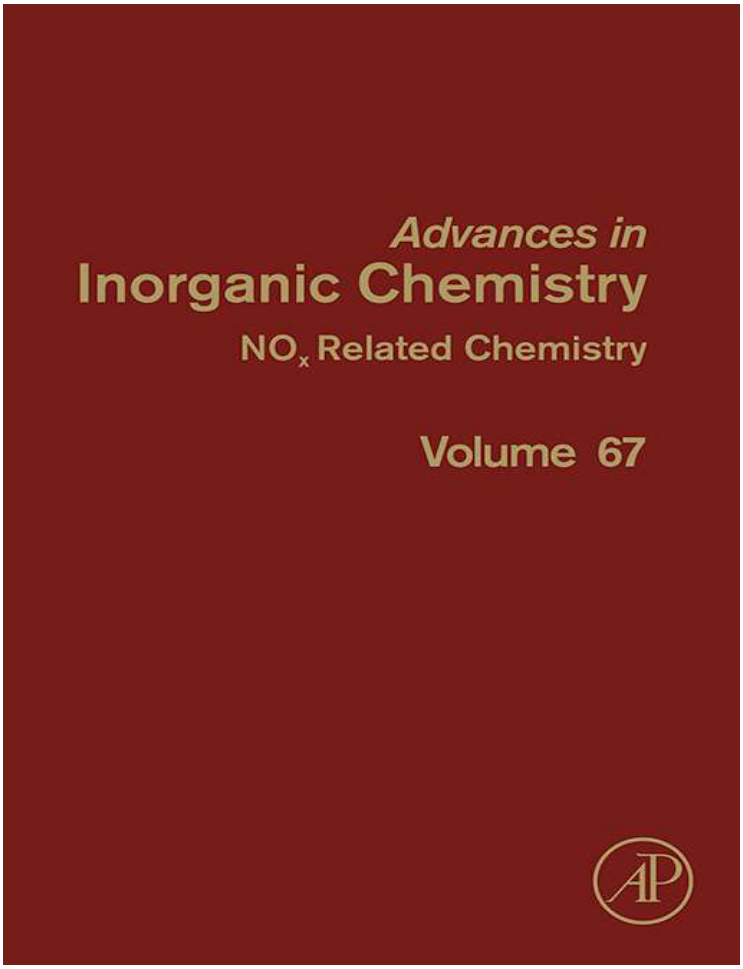

From Sara E. Bari, José A. Olabe and Leonardo D. Slep, Three Redox States of Metallonitrosyls in Aqueous Solution. In: Rudi van Eldik and José A. Olabe, editors, *Advances in Inorganic Chemistry, Vol. 67*, Burlington: Academic Press, 2015, pp. 87-144.
ISBN: 978-0-12-801735-7

CHAPTER TWO

Three Redox States of Metallonitrosyls in Aqueous Solution

Sara E. Bari, José A. Olabe[1], Leonardo D. Slep[1]
Departamento de Química Inorgánica, Analítica y Química Física and INQUIMAE, Universidad de Buenos Aires/CONICET, Facultad de Ciencias Exactas y Naturales, Pabellón 2, Ciudad Universitaria, C1428EHA, Autonomous City of Buenos Aires, Argentina
[1]Corresponding authors: e-mail address: olabe@qi.fcen.uba.ar; slep@qi.fcen.uba.ar

Contents

Abstract

This contribution deals with the structure and reactivity of bound nitrosyl in transition-metal centers (group 8: Fe, Ru, Os). The focus is set on pseudooctahedral nitrosyl-complexes

Advances in Inorganic Chemistry, Volume 67
ISSN 0898-8838
http://dx.doi.org/10.1016/bs.adioch.2014.10.001

with coordination number 5 and 6, containing ancillary coligands of both heme- and non-heme type. The discussion is organized in terms of Enemark and Feltham's classification, selecting complexes within the $\{MNO\}^n$ framework ($n = 6$, 7, and 8). The examples have been chosen for a best description of the electronic structures in terms of modern structural, spectroscopical, and computational methodologies. The selected $\{MNO\}^{6,7,8}$ species reflect the occurrence of three redox states of bound nitrosyl, frequently (though not always) described as NO^+, NO, and NO^- for $n = 6$, 7, and 8, respectively. The analysis is centered on the members of a series of complexes for which the three redox states have been observed on the same platform, viz., $[Fe(CN)_5(NO)]^{2,3,4-}$ and $[Ru(Me_3[9]aneN_3)(bpy)(NO)]^{3,2,1+}$, in aqueous solutions. The influence of the donor–acceptor character of the coligands is specifically addressed with emphasis on the ligand *trans*- to nitrosyl, showing that the latter group may exert a delabilizing influence (as NO^+), as well as a labilizing one ($NO^- \gg NO$) on the *trans*-ligand. On the other hand, typical electrophilic reactivity patterns (toward different nucleophiles) are analyzed for M–NO^+, and nucleophilic reactivity (with O_2) is described for the reduced species, M–NO and M–(NO^-). In the latter case, protonation is described by characterizing the bound HNO species. Important differences are highlighted in the chemistry of bound NO^- and HNO, revealing the strong and mild reductant abilities of these species, respectively. The chemistry is analyzed in terms of the biological relevance to the behavior of nitrite- and NO-reductases and other NO-related enzymes.

1. INTRODUCTION: GENERAL SCOPE

It has been already 40 years since Enemark and Feltham provided a comprehensive description of the structure and bonding of metallonitrosyls, including some reactivity properties. The use of molecular orbital (MO) theory with emphasis in the covalent nature of the bonds led to the $\{MNO\}^n$ description (n is the sum of metal d- and nitrosyl π^* electrons), where the MNO moiety played the role of a functional group while the ancillary coligands became a perturbation *(1)*. This new electron counting $\{MNO\}^n$ formalism allowed organizing in a meaningful classification the available structural data on mononitrosyl-, dinitrosyl-, bridging-, and polynuclear nitrosyls *(2)*. Moreover, this description traced a new direction for reviewing the qualified work in the subject and for dealing with the emerging role of NO in biological functions relevant in neuroscience, physiology, and immunology *(3–6)*. In this context, the role of three redox states of aqueous nitrosyl, namely NO^+, $NO^\bullet$, and NO^- in accomplishing different biological functions by reacting with substrates (O_2, O_2^-, H_2O_2, amines, thiolates, transition metals, and others) has been highlighted *(4)*. These

potential reactivity modes fueled up the research dealing with the changes in the structure and reactivity of nitrosyls upon coordination but emphasising on its "noninnocent" *(7)* character.

We aim to account for our most significant contributions on the metallonitrosyls of group 8 along the past decade, which deal mainly with selected nonheme model complexes in aqueous media. We focus on those systems that share the same coligand-platform for the three $\{MNO\}^{6,7,8}$ redox states (M = Fe, Ru). For iron, we have taken advantage of the distinguished history of the biorelevant sodium nitroprusside (SNP) *(8,9)*. $[Fe(CN)_5(NO)]^{2-}$ is an $n = 6$ species that allowed us exploring the chemistry of the 1-electron reduced $[Fe(CN)_5(NO)]^{3-}$ ($n = 7$) *(10–12)* and of $[Fe(CN)_5(L)]^{n-}$ ($L = NO^-/HNO$), the 2-electron reduced products ($n = 8$) *(12–14)*. For ruthenium, we have accessed to three $\{RuNO\}^{6,7,8}$ analogs containing the $[Ru(Me_3[9]aneN_3)(bpy)]^{2+}$ fragment, thus characterizing not only NO^+, $NO^\bullet$, NO^- but also HNO and NO_2^- as ligands *(15)*. Most significantly, the determinations of pK_as for the $^1HNO/^1NO^-$ conversions in the corresponding $n = 8$ systems opened a new prospect for uncovering the stability range and the reactivity of these largely unknown species in aqueous solutions *(16,17)*.

All along this work, we compare the chemistry of nonheme and heme-metallonitrosyls supported by modern spectroscopic, kinetic, and computational tools, seeking for a unified description of bonding and thermal reactivity and a more precise representation of the electronic structures beyond the Enemark–Feltham classification *(18)*.

2. COMPLEXES WITH $n = 6$

2.1. Structure, spectroscopy, and electronic description. Total spin $S = 0$. Dominant M–NO^+ distribution

Table 1 collects selected metric parameters and IR stretching frequencies (υ_{NO}) for a representative set of six-coordinated (6C) complexes of iron, ruthenium, and osmium, and few iron 5C-compounds. A number of Fe(III) heme proteins are involved in the regulation of the NO biosynthesis by the enzyme NO synthase, in NO transport (as vasodilator) in nitrophorins and in NO inhibition processes of cytochrome P450 and related enzymes *(45)*. Heme enzymes are also intermediates in cyt *cd*1 nitrite reductases (NIRs), *(46)* and in NO reduction by a fungal cyt P450 NO reductase *(47)*. The nonheme Fe(III) nitrile hydratase enzyme (NHase) is relevant to the microbial assimilation of organic nitriles, using

Table 1 Selected list of 6C and 5C nonheme- and heme-nitrosyl complexes $\{MNO\}^6$ (M = Fe, Ru, Os; $S = 0$)

	Compound	ν_{NO} (cm^{-1})	d_{M-N} (Å)	d_{N-O} (Å)	$\angle_{MNO}$ (deg)	Ref.
6C	$Na_2[Fe(CN)_5(NO)]\cdot 2H_2O$	1945	1.6656(7)	1.1331(10)	176.03 (7)	*(19)*
	$[Fe(pyN_4)(NO)]Br_2$	1926	1.67	1.12	179–180	*(20)*
	$[Fe(PaPy_3)(NO)](ClO_4)_2$	1919	1.677(2)	1.139(3)	173.1(2)	*(21)*
	$[Fe(OEP)(2\text{-}MI)(NO)]ClO_4$	1917	1.649(2)	1.132(3)	175.6(2)	*(22)*
	$Fe(TPP)(NO)(O_2CCF_3)$	1907	1.618(8)	1.151(8)	175.8(6)	*(23)*
	$[Fe(cyclam\text{-}ac)NO](PF_6)_2$	1904	1.663(4)	1.132(5)	175.5(3)	*(24)*
	$[Fe(TPP)(H_2O)(NO)]SO_3CF_3$	1897	1.63	1.15	173.0(3)	*(25)*
	$[Fe(`pyS_4')(NO)]PF_6$	1893	1.634(3)	1.141(3)	179.5(3)	*(26)*
	$Fe(OEP)(S\text{-}2,6\text{-}(CF_3CONH_2)_2C_6H_3)(NO)$	1839	1.671(9)	1.187(9)	159.6(8)	*(27)*
	$[FeS_2^{Me2}N_3(Pr,Pr)(NO)]^+$	1822	1.676(3)	1.161(4)	172.3(3)	*(28)*
	$Fe(OEP)(p\text{-}C_6H_4F)(NO)$	1791	1.728(2)	1.153(3)	157.4(2)	*(29)*
	$[Ru(tpm)(bpy)(NO)](ClO_4)_3$	1959	1.774	1.093	179.1	*(30)*
	$[Ru(Me_3[9]aneS_3)(bpy)(NO)](ClO_4)_3$	1945	1.766(4)	1.127(5)	176.5(4)	*(31)*
	$Na_2[Ru(CN)_5(NO)]\cdot 2H_2O$	1926	1.776(5)	1.127(6)	173.9(5)	*(32)*
	$t\text{-}[Ru(NH_3)_4(OH_2)(NO)]Cl_3\cdot H_2O$	1912	1.715(5)	1.142(7)	178.1(5)	*(33)*
	$[Ru(Me_3[9]aneN_3)(bpy)(NO)](ClO_4)_3$	1899	1.768(4)	1.135(5)	172.5(4)	*(15)*
	$[Ru(Papy_3)(NO)](BF_4)_2$	1899	1.779(2)	1.142(3)	170.9(2)	*(34)*
	$[Ru(TPP)(OH_2)(NO)]BF_4\cdot 2H_2O$	1875	1.726(3)	1.143(4)	178.1(3)	*(35)*
	$[Ru(trpy)(\eta^2\text{-}phpy)(NO)](PF_6)_2$	1858	1.826(4)	1.139(5)	167.1(4)	*(36)*
	$t\text{-}[Ru(NH_3)_4(OH)(NO)]^{2+}$	1834	1.735(3)	1.159(5)	173.8(3)	*(37)*
	$t\text{-}[Ru(DMAP)_4(OH)(NO)](BF_4)_2$	1832	1.773(3)	1.245(8)	169.3(6)	*(38)*

Table 1 Selected list of 6C and 5C nonheme- and heme-nitrosyl complexes $\{MNO\}^6$ (M = Fe, Ru, Os; $S = 0$)—cont'd

	Compound	ν_{NO} (cm^{-1})	d_{M-N} (Å)	d_{N-O} (Å)	$\angle_{MNO}$ (deg)	Ref.
	Ru(OEP)(NO)(*p*-C_6H_6F)	1759	1.807(3)	1.146(4)	154.9(3)	*(39)*
	[Ru(T(*p*-OMe)PP)(NO)Et]	1724	1.825(5)	1.139(6)	153.4(5)	*(40)*
	$Na_2[Os(CN)_5(NO)]\cdot 2H_2O$	1897	1.774(8)	1.14(1)	175.5(7)	*(41)*
	[Os(OEP)(NO)(SEt)]	1759	1.994(10)	1.136(11)	172.7(8)	*(42)*
	[Os(OEP)(NO)(OEt)]	1759	1.880(7)	1.165(9)	172.4 (10)	*(42)*
5C-(sp)	[Fe(OEP)(NO)] $ClO_4\cdot CHCl_3$	1868	1.644(3)	1.112(4)	176.9(3)	*(43)*
	[Fe(OEP)(NO)]ClO_4	1838	1.653(1)	1.140(2)	173.2(1)	*(43)*
	[Fe(*S*,SO_2-C_7H_4)(*S*,*S*-C_7H_4)(NO)]$^-$	1761	1.622(5)	1.162(6)	171.9(5)	*(44)*

Nitrosyl stretching frequencies (ν_{NO}) and relevant distances and angles have been detailed.
Abbreviations: bpy = 2,2′-bipyridine; cyclam-ac = 1,4,8,11-tetraazacyclotetradecane-1-acetate pentaanion; DMAP = 4-(dimethylamino)pyridine; 2-MI = 2-methylimidazole; Me_3[9]$aneN_3$ = 1,4,7-trimethyl-1,4,7-triazacyclononane; Me_3[9]$aneS_3$ = 1,4,7-trithiacyclononane; OEt = ethyl oxide; OEP = octaethylporphyrin dianion; $PaPy_3$ = *N*,*N*-bis(2-pyridylmethyl)amine-*N*-ethyl-2-pyridine-2-carboxamide monoanion; phpy = 2-phenylpyridine; pyN_4 = 2,6-C_5H_3N[$CMe(CH_2NH_2)_2]_2$; 'pyS_4' = 2,6-bis-(2-mercaptophenylthiomethyl)pyridine dianion; SEt = ethyl thiolate; 5,5-tpm = tris(1-pyrazolyl) methane; TPP = 5,10,15,20-tetraphenylporphyrin dianion; T(*p*-OMe)PP = tetrakis-(4-methoxy)phenyl porphyrinato; trpy = 2,2′:6′,2″-terpyridine.

NO-uptake and photorelease as regulatory factors *(48)*. Prominent model nonheme iron-nitrosylated species are SNP *(8,9)*, diverse types of dinitrosyls *(49)*, and sulfur clusters (such as Roussin's salts) *(49,50)*, as well as NHase-mimics *(51,52)*. Structural advances have been achieved for the heme-nitrosyl compounds during the last decade *(18,53)*.

2.1.1 Significance and importance of the "back-bonding model"

Figure 1A shows a simplified picture of the arrangement of MOs in 6C $\{MNO\}^6$ linear complexes. The $d\pi$–π^*_{NO} back-bonding model describes the linearity in the MNO units and the multiple character of the Fe–NO and N–O bonds in terms of the orbital mixing of two fully occupied d_π-bonding (d_{xz},d_{yz}) and vacant π^*_{NO} antibonding orbitals, with a minor contribution of the Fe–NO σ-interaction *(4–6)*. The strong electron-acceptor NO^+ gets in this way involved in partial transfer of charge density

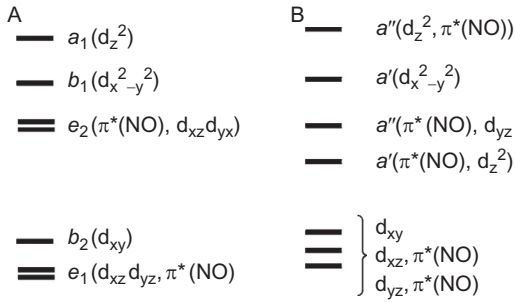

Figure 1 Arrangement of molecular orbitals in $\{MNO\}^n$ complexes, with: (A) $n=6$, linear M–N–O moiety and (B) $n=7$–8, angular M–N–O fragment.

from the metal, thus lowering υ_{NO} from 2390 cm^{-1} in free NO^+ to ~1900 cm^{-1} in the $n=6$ complexes. In turn, the multiple Fe–N bond character becomes reflected in a comparatively high value for υ_{Fe-NO}, at ~590 cm^{-1} *(45)*.

Table 1 shows that most *if not all* of the metallonitrosyls *approach* linearity (170–177° for the MNO angle). At the same time, the M–NO and NO bond lengths reveal multiple characters while the values of υ_{NO} remain comparatively high at ~1900–1950 cm^{-1}. A similar picture arises for iron proteins with N-binding imidazolic *trans*-ligands, like metMb, *cd*1 NIR, and nitrophorin 1 *(45)*. The MNO angles range extends down to ~150°, in parallel with decreasing values of υ_{NO} that reach ~1800 cm^{-1}. It is worth mentioning a heme-thiolate model that exhibits a FeNO angle of ~160° *(27)* and ν_{NO} at 1839 cm^{-1}, very close to values found for the NO-bound ferric P450nor containing *trans*-cysteine *(54)*. Similar results were reported for a model of the inactive form of NH_{ase} with a *trans*-SR^- ligand to nitrosyl *(28)*. The *trans*-SR^- examples (for which also υ_{Fe-NO} becomes lower, ~530 cm^{-1}) suggest that the bending of the FeNO group has an electronic rather than a steric origin *(55)*. In general, the deviations from the typical FeNO angle range occur for complexes with donor ligands (SR^-, OH^-, Cl^-, ONO^-, Et, *p*-C_6H_4F, η^2-phpy, DMAP), occupying mostly axial positions *trans* to the NO group, though there are also examples in the equatorial plane. In the nonheme series of *trans*-$[Ru(NH_3)_4(L)(NO)]^{n+}$, changing $L=H_2O$ by OH^- leads to significant elongations of the Ru–NO and N–O distances (as well as a big shortening of the Ru–O bond), together with a decrease in the RuNO angle and a notorious decrease of υ_{NO} of ~80 cm^{-1} *(33,37,56)*, highlighting the *trans*-weakening role of OH^- on the MNO unit, as discussed for SR^- and other Ls. Overall, the evidence shows similar trends for the group 8 metallonitrosyls, in both heme- and

nonheme systems. The wide range of decreasing υ_{NO}s in Table 1 indicates a decrease in the "nitrosonium" character of the NO ligand, comprising more electron density transfer from the metal to the nitrosyl group (i.e., a partial loss of the triple bond character of free NO^+), within the same Enemark–Feltham $\{MNO\}^6$ category.

Vibrational-spectroscopy has been suggested as a powerful diagnostic tool of the "back-bonding" model for describing the geometry and metric data in the FeNO units. The analysis relies on the *inverse* correlation observed between the values of υ_{FeNO} and υ_{NO} in response to the changes in structure and ligand environment *(45)*, as also described with the metallocarbonyls. By introducing electron-donor substituents in the coligands, υ_{Fe-NO} and υ_{NO} increase and decrease as a consequence of the population of π-(bonding) and π*-(antibonding) orbitals, respectively. The 5C heme-compound $[Fe(OEP)(NO)]ClO_4$ *(43)* appeared as an outlier to this trend as resonance Raman (RR) measurements as well as DFT computations involving several OEP-substituted species suggested a *direct* correlation between υ_{FeNO} and υ_{NO}. It was concluded that the orbitals close to the HOMO were different from those of the analogous CO-complexes. The HOMO itself was described as σ-antibonding with respect to the entire FeNO unit, suggesting a new feature in the bonding picture of the metallonitrosyls. The HOMO-1 and HOMO-2 comprised a degenerate pair, π-bonding with respect to Fe–NO and π-antibonding with respect to N–O, as predicted by the "back-bonding model." Though restricted to the 5C example, this analysis was illuminating for future improvements in the best description of the Fe–N–O bonds.

2.1.2 Role of the σ*-FeNO interaction in the trans-effect exerted over NO

Table 1 shows recent metric parameters for the heme-nitrosyls $[Fe(TPP)(NO)(OC(=O)CF_3)]$ *(23)* and $[Fe(TPP)(NO)(H_2O)]SO_3CF_3$ *(25)*. Both species contain O-binding ligands *trans*- to NO, and apparently behave as typical $Fe^{II}NO^+$ systems. In both cases, the {FeNO} moiety shows a slight bending. It has been suggested that this deviation is due to inherent electronic properties of the species and is not the result of steric restraints imposed by packing of the lattice *(23)*. The coincidence between the experimental and computed FeNO angle at 175.8° for $[Fe(TPP)(NO)(OC(=O)CF_3)]$ reinforces this statement. Additional DFT computations (BP86/TZVP) with a series of [Fe(por)(NO)(L)] complexes containing variable axial anionic Ls with N-, O-, and S-binding atoms, as well as with

neutral methylimidazole (MeIm), actually show that the stronger the donation ability from the axial anionic ligand (namely, $SPh^- > NO_2^- > OC(=O)CH_3^- > OC(=O)CF_3^-$), the weaker the Fe–NO and N–O bonds become and the more the Fe–N–O units bend. The calculated Fe–NO and N–O force constants, frequencies, and FeNO angles agree with this trend. The bending correlates with an increased backbonding into a σ* fully FeNO antibonding orbital, which is unoccupied in the Im-complex but becomes partially filled for complexes with donor axial ligands, by admixture into the occupied MO that results from the bonding interaction of the σ-donor orbital of the ligand and d_{z2} of iron.

2.1.3 *"Negative"* trans*-influence of the nitrosyl moiety*

The nitrosyl ligand affects in different ways the M–L bond lengths of the remaining coligands. For instance, in the nitroprusside dianion the axial Fe–C distance is shorter than the equatorial ones by ~0.05 Å (the axial C–N is also shorter by 0.01 Å) *(19)*. Similarly, the distance to the *N*-carboxamido *trans*-arm in $[Fe(Papy_3)(NO)]^{2+}$, 1.90 Å *(21)*, is significantly shorter than in the related carbonyl analog complex, 1.94 Å *(57)*, as is also the case with the Fe–N(py) distances in the $[Fe(pyS_4)(NO)]^+$ and $[Fe(pyS_4)(CO)]$ complexes, at 2.005 and 2.014 Å, respectively *(26,58)*. A decrease of 0.05 Å has also been measured for the Ru–N distance (*trans* to nitrosyl) in the $[Ru(Me_3[9]aneN_3)(bpy)(NO)]^{3+}$ ion, compared to the one in the corresponding nitro-complex *(15)*. Also, for *trans*-$[Ru(DMAP)_4(NO)(OH)]^{2+}$ *(38)* the Ru–OH distance was the shortest (1.92 Å) among other ruthenium-nitrosyls with OH^- in *trans*-positions, making a difference of ~0.10 Å with the estimated covalent radii at 1.99–2.10 Å *(37,59)*. The comparison of *cis*- and *trans* Ru–L distances for the pentaammino- and pentachloro-nitrosyl ruthenium-complexes *(37,60)* already suggested that the strengthening of the *trans* M^{II}–L bonds to the nitrosyl group is a generalized phenomenon for $n = 6$ complexes. These observations are not privative to nonheme systems: for instance, both in $[Fe(TPP)(NO)(OC(=O)CF_3)]$ and $[Fe(TPP)(NO)(H_2O)]SO_3CF_3$, the Fe–O bonds are 0.03–0.05 Å *shorter* than in the precursors *(23,25)*.

The strong electron-withdrawing power of NO^+, in conjunction with the σ/π-*trans* L-donor abilities, contrasts with the L-*trans* weakening effect promoted by bound-$NO^\bullet$ in the $n = 7$ systems: d_{Fe-L} in $[Fe(Papy_3)(NO^\bullet)]^+$, 1.96 Å *(21)*; $[Fe(pyS_4)(NO^\bullet)]$, 2.167 Å *(26)*, as well as the even stronger effects for the $n = 8$ complexes containing NO^- (see below).

2.1.4 Different reactivity of the L ligand trans to NO

A chemical consequence of the influence of bound-NO^+ is the decrease in the pK_as of the *trans*-ligands, compared with the pK_as in the absence of NO^+. For *trans*-$[Ru(NH_3)_4(H_2O)(NO)]^{3+}$, the $pK_{a(H2O)}$, 3.1, is close to the one measured for the $[Ru^{III}(NH_3)_5(H_2O)]^{3+}$ ion, 4.4, indicating that the $Ru^{II}NO^+$ fragment approaches the behavior of a Ru^{III} center *(33,56)*. Additionally, the water ligand is much more inert toward substitution than in related, non-nitrosylated aqua-complexes *(33,56)*. On the other hand, deprotonation of the *trans*-H_2O ligand induces significant kinetic and mechanistic changes in the nitrosylation/denitrosylation reactions of iron-heme model complexes *(61)*. As a consequence of the discussion presented in Section 2.1.2, NO is expected to be released faster from the bent complexes than from the linear ones, due to the weakening of the Fe–NO bonds.

2.1.5 Other metal centers: Validity of the formal charge descriptions

The electronic structures of manganese-nitrosyls may be discussed on similar grounds as for iron *(18)*. Diamagnetic nonheme complexes show quasi-linear low-spin MnNO fragments, multiple Mn–NO and N–O bonding, and υ_{NO} ~1700–1800 cm^{-1}, in agreement with a stronger π-donor character of Mn in the $\{MnNO\}^6$ fragments, formally described as Mn^INO^+. DFT calculations and RR results support this electronic distribution in $[Mn(Papy_3)(NO)]ClO_4$*(62)*, modifying the previous assignment as $Mn^{II}NO^{\bullet}$*(63)*. A high-spin trigonal bipyramidal (with NO in the equatorial plane) $Mn^{III}NO^-$ ($S=2$) state has been proposed for the 5C [Mn(TC-5,5)(NO)] complex on the basis of IR spectroscopy ($\nu_{NO}=1662\ cm^{-1}$) and SQUID susceptometry *(64)*. For the linear isoelectronic $[M(CN)_5NO]^{n-}$ ions (M = Fe, Mn, V) *(65)* with multiple MNO bond character, υ_{NO} depends strongly on the metal center: 1939, 1725, and 1575 cm^{-1}, with M formally described as Fe^{II}, Mn^I, and V^{-1}, respectively. The large decrease in υ_{NO}s correlated with the increased back-bonding. As the π^*_{NO} character in the HOMO increased from Fe (25%), to Mn (42%), to V (74%), the dominant M(NO^+)-description may be acceptable for Fe^{II}, doubtful for Mn^I, and certainly inconsistent for V^{-1}, for which a $(\pi^*_{NO})^4d^2$ formal structure was suggested. A generalized computational analysis on the electronic structures of tetragonal nitrido- and nitrosyl metal complexes (covering group 7 and 8 metals and ammine/cyanide coligands) maintains an open scenario for best describing the ground state (GS) and lower excited states of metallonitrosyls *(66)*.

2.1.6 Frontier MOs

Early MO calculations provided the composition of the frontier MOs and the character of the electronic transitions in different metallonitrosyls. Briefly, the HOMO has been described as metal-centered for SNP (~65–70%) *(67)* and for many other systems *(45)*. However, in the series of *trans*-$[Ru(NH_3)_4(NO)(L)]^{n+}$ complexes, the HOMO is still metal centered for L = NH_3, H_2O, Cl^-, and OH^-, though it is mainly py- or pz-centered for the N-heterocyclic ligands *(68)*. For the $[Ru(Me_3[9]aneN_3)(bpy)(NO)]^{3+}$ ion (Table 1), a combined experimental UV–vis/(TD)DFT approach allowed assigning the detailed ordering of frontier orbitals *(15)*, with the HOMO defined as a π(bpy) orbital. On the other hand, the LUMO and LUMO + 1 are mostly located on the nitrosyl moiety with ~27% contribution from metal center orbitals, reflecting a substantial π-backbonding, comparable to the one calculated in $[Ru(tpm)(bpy)(NO)]^{3+}$ (25–30%) *(30)* and $[Ru(DMAP)_4(OH)(NO)]^{2+}$ (30%) *(38)*. As a comparison, recent calculations with $[Fe(por)(MI)(NO)]^+$ afforded a pair of LUMO and LUMO + 1 orbitals with composition close to 68% π^*_x,π_y^* and 27% d_{xz},d_{yz} *(69)*.

2.2. Formation and dissociation of NO-complexes: Nitrosylations and denitrosylations

n = 6 metallonitrosyls may be obtained from both M(II) or M(III) precursors by reacting with NO_2^- or NO, respectively, in a pH-controlled medium *(56,70–74)*.

2.2.1 Reactions with M(II) precursors (M = Fe, Ru): Proton-assisted dehydration of bound nitrite

M(II) compounds react with nitrosonium salts in organic media, or with nitrite in aqueous solutions (Equation 1):

$$\left[Fe^{II}\left(X_{eq}\right)_4(L)(H_2O)\right] + NO_2^- + 2H^+ \rightleftarrows \left[Fe^{II}\left(X_{eq}\right)_4(L)(NO)\right]^+ + 2H_2O \quad (1)$$

Reactions like (1) comprise the initial step in the catalytic cycles of some *cd*1 NIRs, implying N-coordination of NO_2^- into the labile (or vacant) Fe(II)-site, followed by the very fast proton-assisted dehydration of NO_2^- (generation of bound NO^+) and reduction/release of NO with formation of the Fe(III)–aqua complex. The latter is reduced by the vicinal heme *c*-reductant (~1 s^{-1}) leading to rebuilding of the catalytic site *(46)*. The reactions like (1) are strongly pH-dependent and are at the heart of

the nucleophilic additions of OH^- into complexes containing the NO^+-ligand (see below).

2.2.2 Reactions with high-spin M(III) precursors

The experimental information for Fe(III) compounds arises mostly from kinetic and mechanistic studies with proteins (metMb, metHb, Cyt^{III}, catalase) and related porphyrinate models *(73,74)* and is specifically addressed in Chapter 4 of this volume. In a general way, the reactions have been described by the equilibrium reaction (2), with L, X, and Y as coligands: L stands for a tetradentate planar ligand, like the porphyrinate derivatives; X is a ligand *trans*- to the NO-binding site; and Y the potentially released ligand, which may be the solvent (eventually, X and Y may be the same).

$$M^{III}L_4XY + NO \rightleftarrows ML_4X(NO) + Y \quad k_{on}, k_{off}, K_{NO} \tag{2}$$

Both the forward (nitrosylation) and reverse (denitrosylation) reactions in (2) are relevant in connection to the potential roles of free and bound NO in biological fluids. The products have been identified as containing the $\{M^{II}NO^+\}$ unit. Therefore, reaction (2) is not a simple ligand substitution but also involves a substantial degree of electronic rearrangement *(61,72)*.

2.2.3 Reactions with low-spin, nonheme Fe(III) systems

These reactions evolve to a full completion, i.e., the reverse reactions are negligible. Consider, for instance, reaction (3) related to the well-studied series of pentacyano(Y)ferrates(III) ($Y = H_2O$, or other ligand) *(75)*

$$\left[Fe^{III}(CN)_5(H_2O)\right]^{2-} + NO \rightarrow \left[Fe(CN)_5(NO)\right]^{2-} + H_2O \tag{3}$$

In this reaction, the nitroprusside dianion (a very stable compound even in aerated aqueous medium) is formed irreversibly. The reverse process in (3), i.e., the release of NO, *only* occurs under light irradiation in the near-UV region *(8,9)*.

A detailed kinetic and mechanistic study of reaction (3) was performed by recording the absorbance decrease of the reactant at 394 and 344 nm. A rigorously linear behavior without intercept was obtained by plotting the pseudo-first-order rate constant, k_{obs}, against [NO], affording a value of $k_3 = 0.25\ M^{-1}\ s^{-1}$ (25.5 °C, pH 3, $I = 0.1$ M) *(76)*. This value is much higher than the one measured in the dissociatively activated complex-formation reactions of $[Fe^{III}(CN)_5(H_2O)]^{2-}$ with nonredox active ligands (k_{on} $\sim 10^{-4}$–$10^{-7}\ M^{-1}\ s^{-1}$) *(75)*. The left part of Figure 2

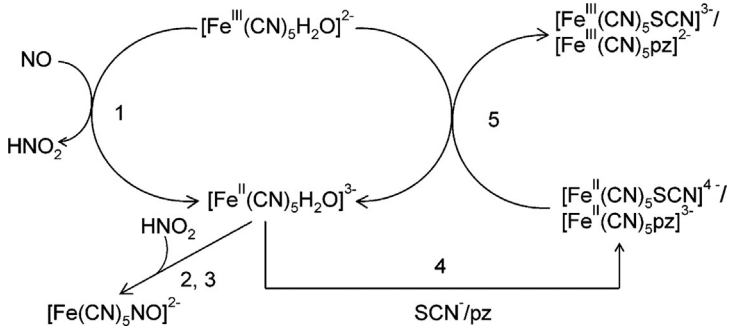

Figure 2 Mechanistic scheme for the reaction between $[Fe^{III}(CN)_5H_2O]^{2-}$ and NO.

(viz., reactions 1–3) highlights the reported mechanistic proposal for reaction (3), described as a rate-determining Fe^{III}-reduction and NO-oxidation to HNO_2 followed by a comparatively faster nitroprusside-formation step. The activation parameters: $\Delta H^{\#} = 52\ \text{kJ mol}^{-1}$, $\Delta S^{\#} = -82\ \text{J K}^{-1}\ \text{mol}^{-1}$, and $\Delta V^{\#} = -13.9\ \text{cm}^3\ \text{mol}^{-1}$ indicate an associative mechanism and were accounted for in terms of the increase in electrostriction due to charge concentration during the electron-transfer process. The redox events in the $NO \rightarrow NO^+ \rightarrow HNO_2/NO_2^- \rightarrow [Fe(CN)_5(NO)]^{2-}$ process involve the onset of very fast proton-assisted NO_2^-/NO^+ interconversions on Fe(II) (see Section 2.2.1).

Importantly, the reduced $[Fe^{II}(CN)_5(H_2O)]^{3-}$ intermediate was detected because of its selective reactivity toward added pyrazine or thiocyanate (cf. reactions 4–5 in the right part of Figure 2), leading to a catalytic mechanism for the consumption of the Fe(III)-reactant. Experimentally, this was revealed by the characteristic spectral changes and the linear dependence of k_{obs} with the concentrations of the scavengers (NCS^- or pz). As suggested in a review *(74)*, the excess NO conditions allow establishing an autocatalytic role for NO, given its binding ability to $[Fe^{II}(CN)_5(H_2O)]^{3-}$ *(10,11)*.

Additional kinetic reports on low-spin M(III) nitrosylations (see below) prompt for an alternative (and common to other compounds) mechanism to accomplish reaction (3). Consider the consecutive processes described by Equations (4–7)

$$\left[Fe^{III}(CN)_5(H_2O)\right]^{2-} + NO \rightleftarrows \left\{\left[Fe^{III}(CN)_5(H_2O)\right]^{2-}, NO\right\} \quad K_{ec} \quad (4)$$

$$\left\{\left[Fe^{III}(CN)_5(H_2O)\right]^{2-}, NO\right\} \rightleftarrows \left\{\left[Fe^{II}(CN)_5(H_2O)\right]^{3-}, NO^+\right\} \quad K_{et} \quad (5)$$

$$\left\{\left[Fe^{II}(CN)_5(H_2O)\right]^{3-}, NO^+\right\} \rightleftarrows \left\{\left[Fe^{II}(CN)_5(NO)\right]^{2-}, H_2O\right\} \quad K_{diss} \tag{6}$$

$$\left\{\left[Fe^{II}(CN)_5(NO)\right]^{2-}, H_2O\right\} \rightarrow \left[Fe^{II}(CN)_5(NO)\right]^{2-} + H_2O \quad K_{pf} \tag{7}$$

Reaction (4) implies a weak associative interaction, erroneously defined previously as of "outer-sphere" type *(76)*. Encounter complexes have been described and characterized in the nitrosylation/denitrosylation reactions of aromatic compounds and were proposed to be inner-sphere adducts containing weakly bound NO *(77)*. They were considered as immediate precursors of transition states for intramolecular electron transfer, as in reaction (5). The equilibrium constants for reactions (6–7) should be high. The ligand interchange within the adduct-complex, reaction (6), is rate-controlled by the cleavage of the Fe^{II}–H_2O bond, coupled to a fast NO^+-coordination. Therefore, for the kinetic analysis, processes (6–7) could be collected into a single kinetic constant k_{-H2O}.

Based on this description, the rate constant for reaction (3) would reflect the onset of two coupled initial equilibria (K_{ec}, K_{et}), followed by the irreversible ligand-interchange reaction, i.e., $k_3 = K_{ec} \times K_{et} \times k_{-H2O}$. From an estimation of $k_{-H2O} \sim 100$–$300\ s^{-1}$ *(75)*, we calculate $K_{ec} \times K_{et} \sim 10^{-3}\ M^{-1}$ in agreement with a low value for K_{et}, which could be anticipated by the redox potentials for the $Fe^{III,II}$ and NO/HNO_2 couples at pH 3 ($E^\circ = 0.37$ and 0.81 V, respectively). As for the expectations on K_{ec}, associative effects might be sometimes significant, as shown below, though not particularly for reaction (4), presumably affording very weak interactions between NO and the bound cyanides.

2.2.4 Nitrosylation of nitrile-hydratase and models

NH_{ase}, an enzyme containing a 6C low-spin Fe(III) site, contains two deprotonated carboxamido nitrogens and three cysteinate sulfurs, one of them *trans* to the labile active site, which binds H_2O or OH^- ligands *(51)*. Laser photolysis studies under excess NO allowed proposing a mechanism for the nitrosylation and *photoinduced* denitrosylation of NH_{ase} *(78)*. The rate constant for NH_{ase} nitrosylation was estimated by detecting the recovery of the inactive (dark) form in excess of NO after a 355-nm laser pulse. By monitoring the time profile of the absorbance change at 370 nm, a pseudo-first-order kinetics was observed at pH 7.5. The plot of k_{obs} (s^{-1}) versus [NO] yielded an asymptotically increase to a limiting

value. Reactions (8–9) were considered, in similar terms as discussed in Section 2.2.2 for $[Fe^{III}(CN)_5(H_2O)]^{2-}$ (reactions 4–6).

$$\left[Fe^{III}NH_{ase}\right]_{active} + NO \rightleftarrows \left\{\left[Fe^{III}NH_{ase}\right], NO\right\} \quad K_8 = k_8/k_{-8} \qquad (8)$$

The "encounter-complex" intermediate in (8) was assumed to contain a weakly trapped NO, subsequently forming the inactive form of the enzyme by means of an irreversible, intramolecular redox- and coupled ligand-interchange reaction (9):

$$\left\{\left[Fe^{III}NH_{ase}\right], NO\right\} \rightarrow \left\{\left[Fe^{II}NH_{ase}(NO^+)\right]_{inactive} \quad k_9 \qquad (9)$$

In the inactive form, a stable nitrosyl-complex is formed, even under aerobic conditions if preserved from the light. From Equations (8) and (9), the decay rate constant is $k_{obs} = K_8 \times k_9\ [NO]/(1 + K_8[NO])$, and K_8 and k_9 were found to be $2.5 \times 10^3\ M^{-1}$ and $14\ s^{-1}$ from the double-reciprocal plot, respectively. Within our proposed generalized model, the value of K_8 appears as much higher than the value estimated for the product of reactions (4–5), suggesting a stronger association in the encounter complex (the value of K_{et} should still be unfavorable for NH_{ase}). By assuming a diffusive formation of the intermediate ($k_8 \sim 10^{10}\ M^{-1}\ s^{-1}$), k_{-8} was estimated as $4.0 \times 10^6\ s^{-1}$. The mechanism implies that light irradiation of the inactive NH_{ase} releases NO from the Fe-center to a trapping site in the protein moiety, yielding an intermediate that might lead back to the reactants. Note that k_{-8} is much larger than k_9, associated with the final coordination of NO^+ into iron, reflecting the lability of the Fe^{II}–H_2O/OH^- active site of the enzyme. As also accepted for other nitrosylations, the product of reaction (9) has been described as $\{Fe^{II}NO^+\}$, as shown by the EPR-silent properties, the value of υ_{NO} at 1854 cm^{-1}, and RR results. Here again, the release of NO can *only* be achieved photochemically, and in this way NH_{ase} recovers the activation ability toward hydrolysis of organic nitriles to amides.

The pentadentate ligand $Papy_3$, with polypyridine- and *N*-carboxamide-type binding arms, has been designed as a model for NH_{ase}*(21)*. Though kinetic studies are not available, the compound binds NO in the dark, reaction (10):

$$\left[Fe^{III}(Papy_3)(NCMe)\right]^{2+} + NO \rightarrow \left[Fe(Papy_3)(NO)\right]^{2+} + NCMe \qquad (10)$$

The EPR-silent $[Fe(Papy_3)(NO)]^{2+}$ complex is very stable, allowing for the preparation of crystalline solids. The NO-release represented by reversing reaction (10) is not available thermally, but it becomes possible upon illumination *(21)*. In a similar way, the compound $[Fe(bpb)(NO)(NO_2)]$ complex was synthesized upon bubbling NO into an oxygen-free acetonitrile solution of the *low-spin* $[Fe^{III}(bpb)(py)_2]^+$ ion (a nonheme planar analog of the iron(III)-porphyrinate) *(57)*. Notice that the high-spin complex $[Fe^{III}(bpb)(Cl)_2]$ did not afford any isolable nitrosyl, a fact that has been employed to propose that the spin state of the iron center of the precursor complex dictates its affinity toward NO.

2.2.5 Nitrosylation of low-spin Fe(III)-heme models, $[Fe^{III}(TMPS)(CN)(H_2O)]^{4-}$ and $[Fe^{III}(TMPS)(CN)_2]^{5-}$

The nitrosylation of $[Fe^{III}(TMPS)(CN)(H_2O)]^{4-}$ (TMPS = meso-tetrakis(2,4,6-trimethyl-3-sulfonatophenyl)porphyrinato) is represented by reaction (11) and was studied under excess NO-conditions *(79)*:

$$\left[Fe^{III}(TMPS)(CN)(H_2O)\right]^{4-} + NO \rightarrow [Fe(TMPS)(CN)(NO)]^{4-} + H_2O \quad (11)$$

At low concentration of NO, k_{obs} (s^{-1}) follows a linear trend against [NO]. From the slope, the authors calculated a second-order rate constant, $k = 8.2 \times 10^3\ M^{-1}\ s^{-1}$. The mechanism was described as an initial reversible equilibrium comprising water-release, followed by a redox coordination step of NO into the Fe(III) complex. Noticeably, the plot showed saturation-like behavior at high [NO], a fact that was ascribed to side reactions. However, this behavior can be interpreted on the same grounds as for NH_{ase} (see Section 2.2.4) yielding values of $K = K_{ec} \times K_{et}$ and k_{NO} of $4.3 \times 10^2\ M^{-1}$ and $22\ s^{-1}$, respectively. The former value allows proposing an initial encounter-complex formation with similar characteristics as in NH_{ase}; the latter one can be consistently traced to k_{-H2O}, implying a fast water-release followed by a fast NO^+-coordination step. The dicyano-complex $[Fe^{III}(TMPS)(CN)_2]^{5-}$ also led to $[Fe(TMPS)(CN)(NO)]^{4-}$, though with an expectedly slower nitrosylation rate. The limiting value of $k_{obs} = 1.54 \times 10^{-2}\ s^{-1}$ (plot of k_{obs} vs. [NO]) was assigned to k_{-CN}, the specific rate constant for cyanide-release, which was independently measured and associated with positive values of the activation entropy and volume (see also Chapter).

2.2.6 Nitrosylations of other $[Fe^{III}(CN)_5(Y)]^{n-}$ complexes

Complementary evidence on the generalized reaction scheme arises from the nitrosylation reactions involving other $[Fe^{III}(CN)_5(Y)]^{n-}$ ions (Y = py, NCS^-, NO_2^-, CN^-), which also pointed to the formation of Fe(II) species as intermediates though with remarkable differences in the relative rates of $[Fe(CN)_5(NO)]^{2-}$ formation *(76)*. Figure 3 shows the spectral changes for the reaction of $[Fe^{III}(CN)_5(py)]^{2-}$ with NO. The initial absorption band at 414 nm (corresponding to $[Fe^{III}(CN)_5(py)]^{2-}$, also absorbing at 368 nm) *(80)* decreases with time, whereas the absorption at 368 nm first increases and then decreases for longer reaction times. A multiwavelength treatment involving factor analysis reveals an intermediate with a band at 364 nm, consistent with the initial formation of $[Fe^{II}(CN)_5(py)]^{3-}$ *(81)*. From the initial decay at 414 nm, a pseudo-first-order rate constant $k_{obs} = 1.4 \times 10^{-4}\ s^{-1}$ can be estimated, which, importantly, has a similar value than the one obtained for the reaction of NO with $[Fe^{III}(CN)_5(H_2O)]^{2-}$. Thus, reactions 4–5 (for $Y = H_2O$) have very similar initial rates than for Y = py (this is also valid for $Y = NCS^-$, not shown), consistent with the fact that all three complexes have very close redox potentials, ~0.4 V (vs. NHE) *(82)*, and that the K_{ec} values should also be expected to be similarly low. In contrast, the rate of nitrosyl-product formation for Y = py is much slower than for $Y = H_2O$, given that in the first case the cleavage of the stronger Fe^{II}-py bond is

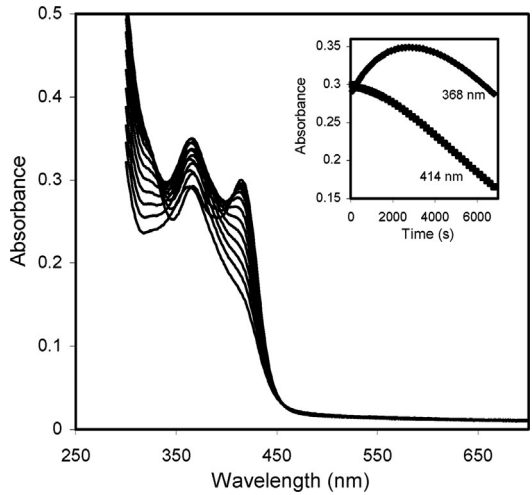

Figure 3 Spectral changes recorded during the reaction of $[Fe^{III}(CN)_5py]^{2-}$ with NO. Experimental conditions: 0.1 mM $[Fe^{III}(CN)_5py]^{2-}$; 0.9 mM [NO]; pH 5.0; 10 mM acetate buffer; $I = 0.1$ M ($NaClO_4$), and cycle time 336 s. Inset: Absorbance-time traces at 414 and 368 nm.

required: in fact, the observed slow subsequent decrease at 368 nm ($k = 1.1 \times 10^{-3}\ s^{-1}$, 25 °C) corresponds to the well-established dissociative aquation rate of the $[Fe^{II}(CN)_5(py)]^{3-}$ ion *(81)*.

The nitrosylation of $[Fe^{III}(CN)_5(NO_2)]^{3-}$ led to a particularly interesting result: a *notoriously fast* conversion to nitroprusside was observed in the stopped-flow time scale. As $E°$ for the $[Fe^{III,II}(CN)_5(NO_2)]^{3,4-}$ couple is also ~0.4 V *(83)*, we can still anticipate similar rates for the encounter-complex formation and the electron transfer reaction steps (analogs of 4–5). However, k_{-NO2-} cannot be high enough to account for the fast conversion to final products (its rate constant should be comparable to k_{-py}, $\sim 10^{-3}\ s^{-1}$). Instead, the final step might involve a fast proton-assisted NO_2^-/NO^+ interconversion (cf. Section 2.2.1), which would yield the product *without rupture* of the initial Fe^{II}–NO_2^- bond:

$$\left\{ \left[Fe^{II}(CN)_5(NO_2)\right]^{4-}, NO^+ \right\}^{3-} \rightleftarrows \left[Fe^{II}(CN)_5(NO)\right]^{2-} + NO_2^- \quad (12)$$

In a nicely significant rate contrast, the reaction of $[Fe^{III}(CN)_6]^{3-}$ with NO was very slow toward the formation of nitroprusside (hours time scale). Again, we expect comparable rates than before for the analogs of reactions (4–5), and a great inertness of the Fe^{II}–CN bond toward dissociation in the $\{[Fe(CN)_6]^{4-}, NO^+\}^{3-}$ intermediate ($k_{-CN} \sim 10^{-7}\ s^{-1}$) *(8)*.

2.2.7 Nitrosylations with Ru(III) precursors

Recent studies on nitrosylation rates of $[Ru^{III}(NH_3)_5(Y)]^{n+}$ ions ($Y = H_2O$, Cl^-, NH_3) *(84)* are described by reaction (13).

$$\left[Ru^{III}(NH_3)_5(Y)\right]^{n+} + NO \rightarrow \left[Ru(NH_3)_5(NO)\right]^{3+} + Y^{n,n-} \quad (13)$$

From the activation parameters, the mechanisms were described as associative bond formations, coupled to concerted electron transfer steps, to produce the same stable nitrosyl ($Ru^{II}NO^+$) complex. A value of $k_{13} = 55\ M^{-1}\ s^{-1}$ was measured for $[Ru^{III}(NH_3)_5(H_2O)]^{3+}$, remarkably faster than for $[Fe^{III}(CN)_5(H_2O)]^{2-}$ (reaction 3). By referring to the general scheme, we consider $k_{13} = K_{ec} \times K_{et} \times k_{-Y}$, and we can estimate the values of k_{-Y} to be in the range $\sim 10^{-2}$ to $6.3\ s^{-1}$ for the different Ys, which means around one or more orders of magnitude faster than the initial electron-transfer step. However, the k_{-Y} values are much smaller than k_{-H2O} in the Fe(III)–aqua complex, $\sim 300\ s^{-1}$. Therefore, the differences in the relative rates of Ru(III) versus Fe(III) nitrosylations should be associated with either K_{ec} or K_{et}. From the redox potentials of the Ru(III) complexes

(∼−0.01–0.06 V), K_{et} is still unfavorable for Ru(III). We conclude that the faster behavior of Ru(III) complexes can be ascribed to a greater K_{ec}, i.e., a stronger association (hydrogen-bonding) ability of NO/NO^+ than in the Fe(III) cyano-complexes.

In the above context, it is worth pointing out that the very fast reactivity ($\sim 10^7\ M^{-1}\ s^{-1}$, pH 7.4) of $[Ru^{III}(edta)(H_2O)]^-$ (leading to $[Ru^{II}(edta)(NO)]^-$) can also be ascribed to its ability for a strong association with the incoming NO *(85)*. The associative character of this reaction seems not to be specific of NO, given that other nonredox active ligands also react very fast with $[Ru^{III}(edta)(H_2O)]^-$ *(86)*.

Timely work from van Eldik's group dealt with the reaction of NO with the *cis*- and *trans*-isomers of $[Ru^{III}(trpy)(NH_3)_2(Cl)]^{2+}$ *(87)*. The mechanistic picture was complex, with faster reactions than for the related Ru^{III}-pentammine systems, and consistent with the more oxidant character induced by the highly acceptor trpy ligand. The initial kinetic behavior showed reversible nitrosylations (NO/Cl^- interchange) for both the *cis*- and *trans*-complexes, with activation parameters compatible with associative processes. In this reaction, the *cis*-$[Ru^{II}(trpy)(NH_3)_2(NO)]^{3+}$ isomer (but not the corresponding *trans*-) was detected by the IR signature of the coordinated NO^+. This species would be formed by a second NO-dependent process, namely an attack of free NO on the initial NO-intermediate. Much slower reactions ($k \sim 10^{-2}\ s^{-1}$ at 55 °C) showing positive activation volumes were assigned to the reactivity of both NO^+-isomers, yielding $[Ru^{II}(trpy)(NH_3)_2(NO_2)]^+$ and $[Ru^{II}(trpy)(NH_3)_2(H_2O)]^{2+}$ due to nucleophilic attack of OH^- followed by aquation, even at pH 2. As free nitrite was quantified at the end of the process only for the *trans*-isomer, it may be inferred that the latter species reacts faster, probably because of its greater $Ru^{II}NO^+/Ru^{II}NO$ redox potential. These processes could be probably included under the general mechanistic scheme comprising encounter-formation steps with a weakly trapped NO that would later evolve to the intermediates of $\{Ru^{II}NO^+\}$ structure.

2.2.8 Why is the release of NO so fast for the $\{Fe^{II}NO^+\}$ heme-nitrosyls?

The products of all the nitrosylation reactions described and analyzed so far for both the heme- or nonheme complexes have been consistently described as diamagnetic low-spin ($Fe^{II}NO^+$) species, independently of the high-spin or low-spin nature of the Fe(III) reactants. Strikingly, there is an evident contrast between the values of k_{off} that measure the lability of NO, between moderately labile heme and the undoubtedly inert nonheme nitrosylated

products *(70)*. The unified heme/nonheme description becomes challenged, because the lability of the heme-nitrosyls is apparently at odds with the strong Fe^{II}–NO^+ bonds appearing *in both types* of nitrosylated model complexes, as well as in heme-proteins. A response to the puzzle has been provided by Lehnert *et al.*, by calculating the potential energy surfaces for the binding of NO to ferric hemes *(69)*. The calculations indicate that the weakness of the Fe–NO bond is not a property of the GS of these complexes, but relates to the existence of a low-lying high-spin state ($S=2$) with Fe(III)–$NO^{\bullet}$ character, dissociative with respect to the Fe–NO bond. Hence, the $n=6$ heme-nitrosyls would be all intrinsically labile because it is expected that this state will always be present at low energy in the different systems. Interestingly, the calculations also identified another state with $Fe^{III}NO^{\bullet}$ character ($S=0$) lying close to the GS ($Fe^{II}NO^+$), though not dissociative. In fact, the singlet $Fe^{III}NO^{\bullet}$ state can be populated by light-irradiation and is believed to be the precursor of NO-photorelease from SNP and other $n=6$ complexes *(8,88)*.

2.3. Electrophilic reactivity toward O-, N-, and S-binding nucleophiles

2.3.1 General approach to electrophilic reactivity

The electron-withdrawing ability of the (formally) NO^+ ligand anticipates the onset of electrophilic reactivity toward external reagents. Theoretical calculations have shown that the N-atom in the delocalized LUMO of the MNO moieties is the site for nucleophilic attack, due to its greater positive charge density *(89)*. This type of reactions, mainly with B nucleophiles such as OH^-, N-bound species as NH_3 and amines, NH_2OH, N_2H_4, N_3^-, NO_2^-, and S-bound ones like RS^-, HS^-, and SO_3^{2-}, have been much studied in the 1970s *(90)* and later on *(91)*. A thermodynamic approach predominated at that time, looking for equilibrium constants. The reactions have been described as occurring in two-steps:

$$\left[M^{II}L_5NO\right]^x + B^y \rightleftarrows \left\{\left[M^{II}L_5N(O)B\right]\right\}^{x+y} \quad (14)$$

$$\left\{\left[M^{II}L_5N(O)B\right]\right\}^{x+y} \rightarrow \left[M^{II}L_5H_2O\right]^x + \text{nitrosation products} \quad (15)$$

Reaction (14) describes the formation and back-dissociation of adducts in a reversible process. Reaction (15) usually involves a bond-reorganization within the adduct, with oxidation of B and reduction of NO^+, formation of the M(II) aqua-complex, and, in most instances, the evolution of gases (N_2 and/or N_2O), or of some other nitrosated product, depending on the

nucleophile and the initial nitrosyl complex *(91)*. A simple nonredox process is operative in reaction (14) with $B = OH^-$, yielding a nitrous acid intermediate that upon rapid deprotonation becomes a bound nitrite. The latter species may remain stable for some time and be easily detectable, or undergo aquation (releasing free nitrite) with a rate that depends on the $M^{II}L_5$ fragment *(92)*. A more complex picture appears in the reaction between N_2H_4 and $[Fe(CN)_5NO]^{2-}$, with the intermediacy of bound linkage isomers of N_2O, namely the "side-on" and "end-on" species as precursors of N_2O release, together with the formation of NH_3. A comprehensive mechanistic report of this reaction *(93)*, reviewed later *(91)*, allowed disclosing different stoichiometries and mechanistic routes for the adduct decompositions employing labeled ^{15}N SNP and substituted methyl-derivatives of N_2H_4. A related picture arises with the more recently studied addition reactions of N- and O-methylated hydroxylamines *(94)*, extending the early study with NH_2OH *(95)*. Finally, the studies related to the addition of RS^- have also unraveled the structure of the metallo-nitrosothiolate (M-NOSR) intermediate adducts *(96)*, and the corresponding biorelevant decomposition processes that lead to reduced nitrosyl compounds *(97)*. Once more, the $[M(CN)_5NO]^{2-}$ complexes have proven particularly useful. With cysteinate as a nucleophile, 1-electron or 2-electron reduction products have been detected, namely NO and N_2O for M = Fe *(97)* and Ru *(98)*, respectively.

Very recently, we revisited the "Gmelin" reaction of SNP with HS^- by performing a detailed kinetic and mechanistic study in a broad time scale, in the pH-range 8.5–12.5 *(99)*. The experimental evidence led proposing the formation of a first adduct intermediate containing the NOSH ligand, which might deprotonate to yield NOS^- with a pK_a value estimated to be 10. Both species were tentatively characterized by the pH-dependent spectral changes originated in electronic transitions at ~570 and 535 nm for both species, respectively. The 1-electron reduced, EPR-active intermediate $[Fe(CN)_5NO]^{3-}$ has also been identified in the reaction medium, in a pH-dependent equilibrium with the *trans*-labilized 5C $[Fe(CN)_4NO]^{2-}$ (both $n = 7$ species, see below). The final reduction product has been identified as NH_3, together with the formation of N_2O at pHs >11. New experiments at pH 7 provided evidence to question the proposed mechanism of this complex reaction. An alternative proposal involves the intermediate formation and release of the 2-electron reduced species nitroxyl (HNO) *(100)*. A current revision of the mechanism of this important reaction is in order, in view of the enhanced interest inside the

biochemical community on the role of H_2S as a new signaling agent. Indeed, the characterization of $NOSH/NOS^-$ and the effective role of 2-electron reduced intermediates (NO^-/HNO) are very challenging hot issues related to the "cross talk" of NO and H_2S as biological signaling agents *(101)*.

2.3.2 Correlation of nucleophilic rates with $M(NO^+)/M(NO^\bullet)$ redox potentials

A significant contribution in this area has been the measurement of key rate constants, k_{OH}, for the addition of the simplest nucleophile, OH^-, to yield stable nitro-complexes. The study involves a wide group of nitrosylated nonheme MX_5 fragments of group 8 metal centers (mainly ruthenium) and different coligands *(92)*. There is a remarkable correlation between ln k_{OH} and the redox-potential for the nitrosyl centered 1-electron reduction couples, $E_{MNO+/MNO\bullet}$ (M = Fe, Ru, Os) that takes the form of a linear-free-energy-relationship *(92)*. The results for the different species can be grouped into two sets of parallel lines. The displacement to lower values of k_{OH} for the same potential in one of them is probably due to steric restrictions of the tetrapyridine-nitrosyl complexes, an explanation that would also account the lack of reactivity of $[Ru(DMAP)_4(OH)(NO)]^{2+}$ toward OH^- and even HS^- *(38)*. The correlation spans an impressive range larger than 1.0 V in the redox potentials and ~10 orders of magnitude in the values of k_{OH}. This trend seems to be valid for other nucleophiles as well, as shown by a series of ruthenium nitrosyls reacting with cysteine *(98)*, and by the addition-reactivity of nitrite toward several iron nitrosyl-hemes *(102)*. The plot is a powerful predictive tool and can in principle be extended to the reactions with the heme complexes. The consensus regarding these species is that the nitrosylation reactions that lead to $\{Fe^{II}NO^+\}$ may be followed by slower processes, namely: (1) addition of OH^- forming bound NO_2^-, (2) rapid aquation of $[Fe^{II}(por)(L)(NO_2)]^-$ (por = porphyrinate dianion) leading to $[Fe^{II}(por)(H_2O)]$ and free NO_2^-, and (3) very fast binding of excess NO to form the $n = 7$ complex $[Fe^{II}(por)(NO)]$. The overall process described by this sequence is usually called reductive nitrosylation *(103)*. Though the effective identification of $[Fe^{II}(por)(L)(NO_2)]^-$ as an intermediate has never been directly achieved for the heme-systems, the linear dependence of the observed rate constants, k_{obs} (s^{-1}), measured by the buildup of the final product, $[Fe^{II}(por)(NO)]$, allows inferring a value for k_{OH}, the nucleophilic rate constant, related to the observed rate constant by $k_{obs} = k_{OH} \times [OH^-]$ *(103)*. Data for the OH^--additions into $Mb^{II}NO^+$, $Hb^{II}NO^+$, and several heme-nitrosyl models containing TPPS, TMPy,

TMPyP (TPPS = tetra-(4-sulfonato-phenyl)porphinato; TMPy = meso-tetrakis(*N*-methyl-4-pyridyl)-porphyrinato; TMPyP = tetrakis-(1-methyl-pyridinium-4-yl)porphyrin)) *(73,74)*, and Por^{16-}, a highly negatively charged substituted model *(104)*, are consistent with the general trend observed for the nonheme species. The results are encouraging, suggesting that a common reactivity picture holds for the nonheme and heme-metallonitrosyls.

3. COMPLEXES WITH $n = 7$

3.1. Structure, spectroscopy, and electronic descriptions for 5- and 6-coordination. Total spin $S = 1/2$ or 3/2. Alternative $Fe^{II}NO^{\bullet}$, $Fe^{III}NO^{-}$, or $Fe^{I}NO^{+}$ distributions

Addition of 1-electron to the $\{FeNO\}^6$ moieties leads to bending of the FeNO group and lowering of the symmetry environment (Figure 1B). The singly occupied MO (SOMO) is mostly located in one of the splitted $\pi^*_{NO\sigma}$ orbitals that is axially σ-antibonding with respect to the iron d_{z2} orbital and therefore weakens the proximal Fe–L ligand *trans* to the NO. In this way, metallonitrosyl compounds may attain CN 5 or 6, both of which are of important in a biological context. The $\{FeNO\}^7$ Enemark–Feltham description leaves room for a large variation of the electronic structure mediated by metal–ligand covalency *(45)*: the $Fe^{II}NO^{\bullet}$ description may need consideration of partial charge transfer, leading in some cases to $Fe^{III}NO^{-}$ or $Fe^{I}NO^{+}$ limiting contributions to the bonding picture, depending on the 5C/6C situation and (in the latter case) on the properties of the *trans*-L ligand.

3.1.1 Heme and nonheme 5C nitrosyls with $S = 1/2$

The 5C heme-compounds have a general formula [Fe(por)(NO)] in some proteins (HbNO, MbNO, sGCNO; sGC = soluble guanylate cyclase) and model complexes, exhibiting a low-spin GS configuration ($S = 1/2$) *(45)*. The iron is displaced toward the axial NO, with larger displacements for the 5C species (~0.2–0.3 Å) than for the 6C ones (~0.1 Å). The FeNO geometries do not show much variation as a function of the porphyrin ligand and present a temperature-dependent structural rotational disorder. High-resolution crystal structures of model complexes reveal a tilting of the Fe–NO bond vector from the heme normal and an asymmetry of the Fe–N(pyrrole) bond distances *(18)*. Table 2 shows data for α-Hb^{II}–NO, for a typical TPP^{2-} derivative, and for a recently prepared compound with

Table 2 Selected list of 6C and 5C nonheme- and heme-nitrosyl complexes, $[FeNO]^7$

	Compound	S	ν_{NO} (cm^{-1})	d_{M-N} (Å)	d_{N-O} (Å)	$\angle_{MNO}$ (deg)	Ref.
6C	[Fe(T1Et4iPrIP)(OTf)(NO)](OTf)	3/2	1831	1.764(1)	1.150(5)	171.5(4)	*(105)*
	[Fe(^{Me}Tp)(acac^{PhF3})(NO)]	3/2	1720–1761	1.813(3)	1.148(4)	147.7(3)	*(106)*
	[Fe(BMPA-Pr)(Cl)(NO)]	3/2	1726	1.7828(7)	1.1545(9)	151.80(7)	*(107)*
	[Fe(cyclam)$(N_3)_2$(NO)]	3/2	1690	1.738(5)	1.142(7)	155.5(10)	*(108)*
	[Fe(N4py)(NO)]$(BF_4)_2$	1/2	1672	1.732(2)	1.157(3)	144.9(2)	*(109)*
	[Fe(N3PyS)(NO)](BF_4)	1/2	1660	1.7327(18)	1.150(3)	147.2(2)	*(109)*
	[Fe(pyS_4)(NO)]	1/2	1648	1.712(3)	1.211(7)	143.8(5)	*(26)*
	[Fe(TPP)(MI)(NO)]	1/2	1628	1.750(2)	1.182(3)	137.7(2)	*(110)*
	[Fe(pyN_4)(NO)]Br_2	1/2	1620	1.737(6)	1.175(8)	139.4(5)	*(20)*
	[Fe(cyclam-ac)(NO)](PF_6)	1/2	1615	1.722(4)	1.166(6)	148.7(4)	*(24)*
	[Fe$(PaPy_3)$(NO)](ClO_4)	1/2	1613	1.7515(16)	1.190(2)	141.29(15)	*(21)*
	t-[Fe(cyclam)(Cl)(NO)](ClO_4)	1/2	1611	1.820(4)	1.006(4)	144.0(4)	*(111)*
	Na_3[Fe$(CN)_5$(NO)]·$2NH_3$	1/2	1608	1.737	1.162	146.6	*(12,112)*
5C	[Fe(TMC)(NO)]$(BF_4)_2$ (tbp)	3/2	1840	1.737(6)	1.137(6)	177.5(5)	*(113)*
	[Fe($\mathbf{1}^{dmp}$)(NO)]$^-$ (tbp)	3/2	1750	1.748(2)	1.146(3)	160.3(2)	*(114)*
	[Fe($\mathbf{1}^{ipr}$)(NO)]$^-$ (tbp)	3/2	1729	1.735(4)	1.122(5)	178.2(5)	*(114)*
	[Fe(TMG_3tren)(NO)]$(OTf)_2$ (sp)	3/2–1/2	1748	1.748(2)	1.154(3)	168.0(2)	*(115)*

Continued

Table 2 Selected list of 6C and 5C nonheme- and heme-nitrosyl complexes, $[FeNO]^7$—cont'd

Compound	S	ν_{NO} (cm^{-1})	d_{M-N} (Å)	d_{N-O} (Å)	$\angle_{MNO}$ (deg)	Ref.
[Fe(3,5-Me-BAFP)(NO)] (sp)	1/2	1684	1.714(4)	1.142(5)	146.6(4)	*(116)*
$(NEt_4)_2[Fe(CN)_4(NO)]$ (sp)	1/2	1746	1.565	1.161	177.1	*(117)*
[Fe(TC-5,5)(NO)] (tbp)	1/2	1692	1.670(4)	1.176(5)	174.3(4)	*(118)*
α-Hb^{II}–NO (sp)	1/2	1668	1.74	1.1	145	*(119)*
[Fe(bpb)(NO)] (sp)	1/2	1673	1.7129(11)	1.1818(15)	144.74	*(57)*
[Fe(TPP)(NO)] (sp)	1/2	1670(1697)	1.739(6)	1.163(5)	144.4(5)	*(120)*
$[Fe(PhPepS)(NO)]^{2-}$ (sp)	1/2	1626	1.700(2)	1.191(3)	149.3(2)	*(121)*
$[Fe(S,S\text{-}C_6H_2\text{-},6Cl_2)_2(NO)]^{2-}$ (sp)	1/2	1615	1.702(5)	1.186(6)	153.4(4)	*(44)*

Total spin S, nitrosyl stretching frequencies (ν_{NO}), and relevant distances and angles have been detailed.
Abbreviations: $acac^X$ = substituted acetylacetonate; BMPA-Pr = *N*-methylpropanoate-*N*,*N*-bis(2-pyridylmethyl)amine; bpb = dicarboxamide dianion; cyclam- = 1,4,8,11-tetraazacyclotetradecane; Hb = hemoglobin; 3,5-Me-BAFP = 3,5-methyl-bis(aryloxy)-fence porphyrin dianion; N4py = *N*,*N*-bis(2-pyridylmethyl)-(*N*-(bis-2-pyridylmethyl)amine); N3pyS = *N*,*N*-bis(2-pyridylmethyl)-(*N*-(bis-2-pyridylmethyl)amine) with one thiolate-*S*-ligand replacing one of the py donors; OTf = trifluoromethanesulfonate anion (triflate); PhPepS = *N*,*N*′-(1,2-phenylene)bis(2-mercaptobenzamide); TMC = 1,4,8,11-tetramethyl-1,4,8,11-tetraazacyclotetradecane; TMG_3tren = a substituted derivative of tris(2-aminoethyl)amine; ^{Me}Tp = methyltris(pyrazol-1-yl)borate; T1Et4iPrIP = tris(1-ethyl-4-isopropylimidazolyl) phosphine; $\mathbf{1}^{dmp}$ = tris(*N*-(3,5-dimethylphenyl)carbamoylmethyl)amine trianion. See Table 1 for other abbreviations.

a bis-picket fence porphyrinate, 3,5-Me-BAFP^{2-}, which is interesting for being the first compound with a 5C ferrous heme-nitrosyl with a TPP^{2-} derivative as coligand that shows a single conformation of the Fe–NO unit. Most of the heme compounds have Fe–NO distances at ~1.70 Å (expectedly larger than for the $n=6$ systems), and FeNO units at ~145°. Included are data for selected nonheme compounds. The structures are mostly square pyramidal, with bent FeNO geometries as for the heme-nitrosyls, with the exception of the trigonal bipyramidal (tbp) tropocoronand (TC) complex. The [Fe(*S*,*S*-C_6H_2-,$6Cl_2)_2$(NO)]$^{2-}$ anion *(44)* is prototypical of a class of 5C iron complexes containing planar equatorial coligands of the dithiolene family. On the other hand, [Fe$(CN)_4$(NO)]$^{2-}$ originated on the 1-electron reduction followed by cyanide loss of the nitroprusside dianion *(117)* contains a FeNO unit distinctively close to linear with a very short Fe–N bond, 1.56 Å, even shorter than in SNP, 1.67 Å.

Overall, the values of υ_{NO} display a wide range, 1615–1690 cm^{-1}, for the bent systems, with the exception of SNP, 1746 cm^{-1}. The υ_{Fe-NO}s and δ_{FeNO} bendings are at 520–540 and 360–390 cm^{-1}, respectively *(45)*. The latter indicators are increasingly used with heme-proteins in order to sense the environment of the active sites. 5C heme-nitrosyls exhibit characteristic EPR spectra with anisotropic *g*-matrices' principal values close to 2.10, 2.06, and 2.01 *(45)*, similar to [Fe$(CN)_4$(NO)]$^{2-}$ *(117)*.

The nature of the SOMO is relevant for understanding the charge distribution in this kind of species (Figure 1B). For instance, in [Fe(por)(NO)] the mixing between $\pi^*_{NO\sigma}$ and d_{z2} is strong enough to yield a computed net transfer of about half an electron to the iron center, i.e., the unpaired electron of NO is fully delocalized over the FeNO subunit, with calculated spin populations of about +0.5 on Fe and +0.5 on NO. Besides this strong Fe–NO σ-bond, the other vacant π^*_{NO} forms a medium-strong π-backbond with the fully occupied d_{yz} orbital, and an additional π backbond results from the interaction of $\pi^*_{NO\sigma}$ with d_{xz}. In summary, NO behaves as a strong σ-donor and medium-strong π-acceptor in the 5C heme nitrosyls. The strong σ-donation of NO determines a noticeable Fe^{I}–NO^{+} character, i.e., a partial charge transfer (iron reduction/NO oxidation). The strength of the π backbond can be modulated by adding electron withdrawing or donating substituents to the phenyls of TPP^{2-}-type ligands, leading to inverse correlations between υ_{Fe-NO} and υ_{NO} *(45)*. For [Fe$(CN)_4$(NO)]$^{2-}$, a *dominant* Fe^{I}–NO^{+} character is suggested by comparing the metric indicators and the distinctive high values of υ_{NO} and υ_{CN} at 1746 and 2100 cm^{-1}, respectively *(112)*. The results indicate (together with the short Fe–NO

distance) that the strength of both σ/π bonds is synergistically enhanced (low formal charge at Fe^{I}). Finally, [Fe(TC-5,5)(NO)] shows an unusual case of a bipyramidal structure with an equatorial NO. Also unusual for the half-spin systems, an electronic distribution with low-spin $Fe^{III}NO^{-}$ has been proposed on the basis of EPR, Mossbauer, SQUID susceptometry, and normal coordinate analysis *(118)*.

3.1.2 Nonheme and heme 6C nitrosyls with S = 1/2

An experimental and theoretical EPR study of the $[M(CN)_5NO]^{3-}$ anions (M = Fe, Ru, Os) *(122)* showed spectra that are close to axial ($g_{1,2} \sim 2.00$, $g_3 < 2.00$) and one ^{14}N hyperfine coupling constant, suggesting the identification of paramagnetic $[M^{II}(CN)_5NO^{\bullet}]^{3-}$. High-level DFT calculations revealed that the most pronounced changes upon reduction of the $n = 6$ compounds are concentrated in the M–NO lengths and in the MNO angles (close to 145°), with a lowering of symmetry that leads to the removal of degeneracy of the π^*_{NO}. For the three metal centers, the computed compositions of the SOMO show that spin densities are mainly confined to the NO groups, with about two-thirds share on the N-atom, though with sizeable metal contributions. The strongly increasing spin-orbit coupling from Fe < Ru < Os is evident from both the experimental and calculated data and is most pronounced in the Os system where g_3 and the calculated isotropic value g_{av} are lowest and the total anisotropy g_1–g_3 is largest. This work established a firm basis for assigning the EPR spectra of $n = 7$ systems with $S = 1/2$, contributing to a confirmation of the early work with $[Fe^{II}(CN)_5NO]^{3-}$ *(123)*, and allowed discriminating with the 5C $[Fe(CN)_4NO]^{2-}$, which at that time was erroneously reported as $[Fe(CN)_5NOH]^{2-}$. The success of the interpretation has been later extended to a great variety of $[M^{II}L_5NO^{\bullet}]^{x}$ complexes containing coligands that induce relatively strong ligand field situations *(124)*. A comprehensive EPR study was done with the iron containing $[Fe(cyclam\text{-}ac)(NO)]^{+}$ mono-cation, complemented by IR, UV–vis, Mössbauer, and computational methods *(24)*. As an example, Figure 4 shows the EPR spectrum of $[Ru(bpy)(tpm)(NO)]^{2+}$ *(30)*.

Typical g values for 6C heme-nitrosyls are markedly smaller than those for their 5C analogs. Consistently, magnetic circular dichroism (MCD) spectroscopic measurements and DFT calculations *(125)* show a decrease in the spin density on Fe when going from 5C [Fe(TPP)(NO)] to 6C [Fe(TPP)(MI)(NO)]. Other EPR differential features related to the hyperfine splitting pattern have been analyzed in detail in a recent review *(45)*, as is

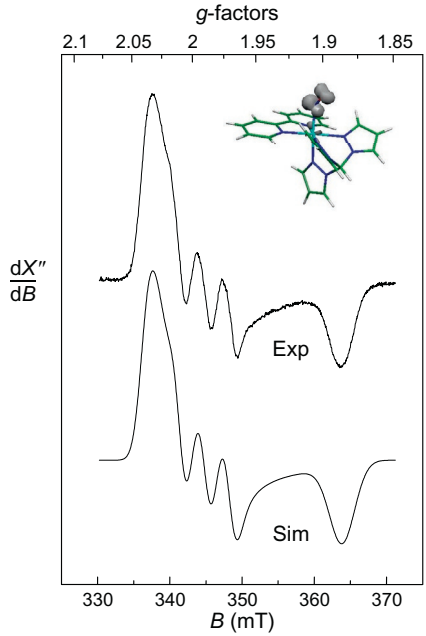

Figure 4 EPR spectrum of the electrogenerated cation $[Ru(bpy)(tpm)NO]^{2+}$ in MeCN/0.1 MBu_4NPF_6 at 110 K. Experimental conditions: microwave frequency, 9.604 GHz; modulation amplitude, 4 G. Bottom: computer-simulated spectrum. Top right: DFT-calculated spin density of the same species in a vacuum (B3LYP level, LanL2DZ basis set).

also the case with the use of vibrational spectroscopy in the low-energy region. Concerning the N–O and Fe–NO bonds, both are simultaneously weakened when going from 5C to 6C. This can be best appreciated by comparing the IR results for the TPP^{2-}-complexes: the decrease of υ_{NO} by 40 cm^{-1} upon coordination of MI is accompanied by a decrease of υ_{Fe-NO} ($520 \rightarrow 440$ cm^{-1}). The direct correlation indicates a weakening of the Fe–NO σ-bond upon coordination of the sixth ligand *(126,127)*. In short, DFT calculations show that the *trans*-binding reduces mixing of the SOMO of NO with the d_{z2} orbital of the Fe center due to an σ-*trans* interaction with the proximal N-donor ligand. Because of the reduced donation from the $\pi^*_{NO\sigma}$ orbital, the N–O bond is also weakened, as is evident from the decrease of υ_{NO}. The spin-density distributions are about +0.8 on NO and +0.2 on iron for the 6C complexes, in contrast with the ~50% distribution in the 5C ones. Therefore, the 6C heme-complexes correspond to a dominant $Fe^{II}NO^{\bullet}$ distribution, in full agreement with the 6C nonheme nitrosyls. Table 2 includes several examples of complexes affording the

above-described electronic structure, as well as recent data on a structural and electronic model of NO-bound cysteine dioxygenase, [Fe(NO)(N3PyS)]BF_4, together with a related all-N donor analogue, [Fe(NO)(N4py)]$(BF_4)_2$ *(109)*.

3.1.3 Nonheme nitrosyls with $S = 3/2$

Some nonheme ferrous centers in metalloproteins *(128)* react reversibly with NO yielding bent 6C nitrosyl species with $S = 3/2$ GSs. EPR, RR, XAFS, MCD, and Mössbauer spectroscopies, together with SQUID susceptometry and theoretical calculations, support a best description as $Fe^{III}NO^-$ (high-spin ferric, $S = 5/2$, antiferromagnetically coupled to NO^-, $S = 1$). Table 2 includes data for an early described nonheme example, [Fe(cyclam)$(N_3)_2$(NO)] *(108)*, and for two recently published models of oxygenase enzymes able to bind NO *(105,106)*. Many other complexes with a low- to medium-field coordination sphere strength have been described in similar terms, namely $[Fe(H_2O)_5(NO)]^{2+}$ *(129)*, [Fe(edta)(NO)] *(130)*, and a series of ferrous chelate nitrosyls containing amino-carboxylate and pyridylmethylamine coligands *(131)*.

Table 2 includes some 5C examples with different geometries. An early work showed the first structurally characterized example of a high-spin $n = 7$ compound, containing TMC, among a few other similarly behaved analogs *(113)*; it contains the NO group in the apical position of a distorted tetragonal pyramid (in fact, intermediate between sqp and tbp) and displays a temperature-dependent spin-equilibrium distribution, 3/2–1/2. Also included are two representative bipyramidal complexes within the series of tripodal ligands derived from tris(*N*-R-carbamoylmethyl)amine. The R groups provide cavities around the metal center that influence the structure and particularly the degree of FeNO bending, with Fe–N–O angles that range from 178.2° (R = ^{i}Pr) to 160.3° (R = dmp). The structural changes are reflected in the EPR spectra that become significantly more rhombic for the highly bent ligands *(114,132)*. These last complexes have been also described as $\{Fe^{III}NO^-\}$ systems. Finally, the recently prepared tbp $[Fe(TMG_3tren)(NO)]^{2+}$ complex *(115)* has shown to be a precursor for the first high-spin nonheme $[FeNO]^8$ complex (see below).

3.2. The *trans*-effect in heme- and nonheme complexes

It has been well established that sGC binds NO to a ferrous heme active site, leading to the intermediate formation of a 6C complex, followed by the breaking of the *trans*-Fe–his bond and generation of a 5C ferrous heme

nitrosyl *(45, 133)*. In histidine heme-model complexes, coordination of NO leads to a substantial weakening of the Fe-imidazole bonds *trans*- to NO, showing binding constants of at most 10–50 M^{-1} *(127)*. Stable 6C ferrous heme-nitrosyls have been obtained for globins containing a restrained axial histidine. For several nonheme nitrosyl-complexes, Tables 1 and 2 allow comparing the distances of the *trans*-ligands for the $n=6$ and 7 systems (cf. examples with the same non-nitrosyl coligand platform), showing a substantial elongation for the $n=7$ case. In aqueous solutions, the magnitude of the *trans*-labilizations may be strongly dependent on the nature of the ligand and on specific situations related either to their pK_as in the aqueous media or to specific environmental effects, namely H-bond associations with N-residues. Thus, the 6C and 5C cyano-nitrosyl complexes equilibrate in aqueous solutions according to:

$$\left[Fe(CN)_5(NO)\right]^{3-} \rightleftarrows \left[Fe(CN)_4(NO)\right]^{2-} + CN^- \quad k_{16}, k_{-16}, K_{16} \qquad (16)$$

Values of $k_{16}=2.7\times10^2\ s^{-1}$, $k_{-16}=4\times10^6\ M^{-1}\ s^{-1}$, and $K_{16}=6.8\times10^{-5}$ M have been measured *(134)*. It can be seen that the "*trans*-effect" translates into a low value of K_{16} (i.e., a high binding constant for the 6C species, in contrast with sGC) suggesting that the "brown" 6C species should be dominant in the currently studied solutions. However, the protonation of cyanide (pK_a(HCN) = 9.3) drives reaction (16) to the right and favors the dominant formation of the 5C "blue" species in neutral solutions. As detailed in the next section, the $[Fe(CN)_4(NO)]^{2-}$ ion may release NO in specific endogenous conditions, leading to sGC activation. Labilization also arises upon 1-electron reduction of $[Ru(NH_3)_5(NO)]^{3+}$, with a subsequent rapid detachment of *trans*-NH_3 *(135)*.

3.3. Formation and dissociation of NO-complexes: Disproportionation reactions

3.3.1 Nitrosylations

Direct mixing of *stoichiometric* NO with M(II) complexes (either 5C or 6C) leads to $\{MNO\}^7$ species:

$$\left[M^{II}L_5(H_2O)\right]^x + NO \rightleftarrows \left[ML_5(NO)\right]^x + H_2O \quad k_{on}, k_{off} \qquad (17)$$

The $\{MNO\}^7$ species can also be generated chemically or electrochemically by reduction/oxidation of adequate precursors. Relevant kinetic and mechanistic information has been provided corresponding to reaction (17), comprising the different electronic distributions for $n=7$, as detailed above.

For the aqua- and chelate-complexes described as $Fe^{III}NO^{-}$ ($S=3/2$, derived from high-spin metal centers), water-exchange measurements and activation parameters support a dissociative-interchange mechanism, with high values of k_{on} and variable values of k_{off} as a function of the type of chelate *(131)*. Dissociative mechanisms have been proposed for the prototypical low-spin $[Fe(CN)_5(NO)]^{3-}$ complex ($S=1/2$, described as $Fe^{II}NO^{\bullet}$), showing much lower values of k_{off} at $\sim 10^{-5}\ s^{-1}$ *(10,11)*. The coordination of NO into the low-spin $[Fe(CN)_5(H_2O)]^{3-}$ ion evolves through a dissociative process, controlled by the lability of the Fe–OH_2 bond, i.e., the values of k_{on} are all around ca. $300\ M^{-1}\ s^{-1}$ for the neutral incoming ligands (viz., NH_3, py, and CO), with smaller/greater values for the negatively/positively charged ones, respectively *(10,11)*. For the porphyrinate models (cf. $[Fe^{II}(TMPS)(H_2O)(NO)]$), much higher values of k_{on} at $\sim 10^{8}\ M^{-1}\ s^{-1}$ are found (high-spin reactants), though the values of k_{off} are low and of the same order as found for the nonhemes *(73,74)*. For the important class of *in situ*-generated, low-spin $[Ru^{II}(NH_3)_4(L)(NO^{\bullet})]^{n+}$ complexes, variable values of k_{off} have been estimated (range $\sim 1–10^{-4}\ s^{-1}$), suggesting the influence of the donor/acceptor abilities of the *trans* L ligands *(56)*.

3.3.2 Dinitrosyl complexes and disproportionation reactions

The conversion of NO into N_2O that takes place at the active sites of NO-reductases has stimulated investigations on the different mechanistic routes to promote NO-coupling. The formation of dinitrosyls or the proposed intermediacy of closely situated NO-species arising from structurally different FeNO-complexes in the route to N_2O-formation are a matter of current interest. For these topics, the reader is referred to recent reviews *(115,136)*. Our contribution in this issue involved a close look at the intrinsic reactivity of $[Fe(CN)_5(NO)]^{3-}$, in the absence and in the presence of an excess of NO conditions, showing an interesting scenario of successive biorelevant reactions *(11)*.

An early concern on the hypotensive properties of solutions of SNP, which manifest readily a few seconds after injection, led to the proposal that reaction (16) is rapidly established once SNP is reduced by the thiolates in the biological medium. Given the inertness of $[Fe(CN)_5(NO)]^{3-}$ toward NO-release *(10)*, the activation of sGC was assigned to the lability of $[Fe(CN)_4(NO)]^{2-}$ *(137)*. As there was no evidence in favor of the latter proposal, we afforded a kinetic and mechanistic study on the thermal decomposition of $[Fe(CN)_5(NO)]^{3-}$ (rapidly generated from SNP upon reduction

by dithionite) under a wide pH-range (4–10), i.e., studying solutions with a pH-controlled ratio of $[Fe(CN)_5(NO)]^{3-}/[Fe(CN)_4(NO)]^{2-}$ *(11)*.

At the left-center of Figure 5, we show the equilibrium mixture of the reactant complexes. At pH 9, a pseudo-first-order decay of predominant $[Fe(CN)_5NO]^{3-}$ can be observed, with $k_{off} = 4 \times 10^{-5}\ s^{-1}$, in fair agreement with the reported value for k_{-NO} *(10)*. NO was formed during the first 15 min and was absent after 10 h. Some N_2O and SNP were observed as minor decomposition products for ca. 10 h of reaction. The onset of a new band at 2038 cm^{-1}, typical of $[Fe(CN)_6]^{4-}$, agrees with Equation (18), describing a process subsequent to NO-dissociation, with successive release/recombination of cyanides *(138)*.

$$\left[Fe(CN)_5H_2O\right]^{3-} \rightarrow \frac{5}{6}\left[Fe(CN)_6\right]^{4-} + \frac{1}{6}Fe^{2+} + H_2O \qquad (18)$$

At pH 6, the consecutive spectra showed the decay of mainly $[Fe(CN)_4NO]^{2-}$ (λ_{max}, 615 nm). The absorbance traces at two selected wavelengths fitted to a two-exponential model. A slow monotonic decay at 615 nm, along with an initial increase and subsequent decrease of an intermediate I_1 with maximum at 336 nm, was observed. Values of $k_{obs} = 3$–6 and 1–$2 \times 10^{-5}\ s^{-1}$ were calculated for the steps involving the formation and decay of I_1, respectively. NO was shown to be generated during the first minutes and decreased slowly with time. A continuous formation of N_2O evolved with $k_{obs} = 1.4 \times 10^{-5}\ s^{-1}$. At the end of the reaction,

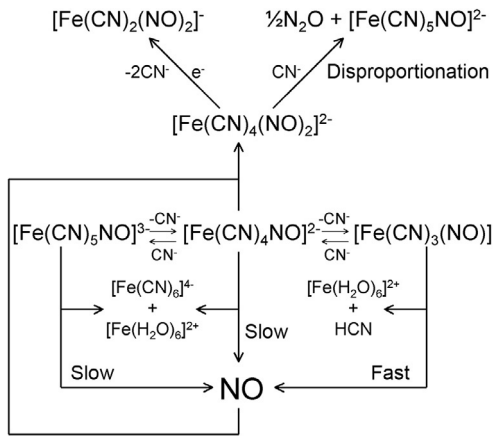

Figure 5 Mechanistic scheme starting with $[Fe^{II}(CN)_5NO]^{3-}$, illustrating the decomposition paths at different pHs.

$[Fe(CN)_6]^{4-}$ was found in low yields, in contrast with high yields of free cyanides. Importantly, a disproportionation reaction led to SNP and N_2O (40% and 20%, respectively, with respect to the initial concentration of $[Fe(CN)_5NO]^{3-}$). The successive IR spectra showed a decreasing intensity of the bands corresponding to $[Fe(CN)_4NO]^{2-}/[Fe(CN)_5NO]^{3-}$, along with an increase in the bands for $[Fe(CN)_6]^{4-}$, SNP, and N_2O. The outstanding feature was the appearance of a transient weak absorption at 1695 cm^{-1} (maximum intensity at ~2.5 h), which was absent at the beginning and at the end of the process, revealing its intermediate character. We assigned this feature to ν_{NO} in I_1, consistent with the UV–vis results and with isotope-labeling measurements with ^{15}NO. In an independent experiment, the IR-peak at 1695 cm^{-1} shows up by adding NO in a controlled way to $[Fe(CN)_4NO]^{2-}$ (with a new, weaker one at ca. 1737 cm^{-1}). Both peaks disappear by adding excess of NO, suggesting that I_1 is unstable under these conditions. Finally, the EPR monitoring measurements showed that the initial signal of the reactants mixture evolves to a different one for a final paramagnetic product (named as I_2, see below), with an EPR-silent intermediate, also assignable to I_1.

We proposed that I_1 is a *trans*-dinitrosyl species formed after NO-dissociation from $[Fe(CN)_4NO]^{2-}$, Equation (19), with subsequent coordination to the same complex (Equation 20):

$$\left[Fe(CN)_4NO\right]^{2-} + 2H_2O \rightleftarrows \left[Fe(CN)_4(H_2O)_2\right]^{2-} + NO \qquad (19)$$

$$\left[Fe(CN)_4NO\right]^{2-} + NO \rightarrow \left[Fe(CN)_4(NO)_2\right]^{2-} \qquad (20)$$

The EPR-silent properties of I_1 were ascribed to a low-spin Fe(II) center containing two antiferromagnetically coupled NO ligands. Independent kinetic results for reaction (20) showed a first-order rate law in each reactant, with $k_{20} = 4.3 \times 10^4\ M^{-1}\ s^{-1}$. Recent reports deal with the coordination of NO to ferrous nitrosyl-porphyrins to yield *trans*-[Fe(por)$(NO)_2$] in low-temperature solutions *(139)*. These are also EPR-silent complexes, with similar IR properties as described for I_1. From theoretical calculations, a *trans*-syn (C_{2v}) conformation has been proposed for [Fe(TPP)$(NO)_2$]. We found a similar picture for $[Fe(CN)_4(NO)_2]^{2-}$, also reproducing the *trans-syn* geometry, with fairly consistent ν_{NO} values.

By lowering the pH to 4, the decomposition of $[Fe(CN)_4NO]^{2-}$ becomes faster by 2 orders of magnitude, with a subsequent release of cyanide, NO, and aqueous Fe(II) ions (right, lower part in Figure 5). The process is favored by the presence of metal ions (Cu, Fe). Therefore, our final

conclusion is that NO requires the previous labilization of more cyanides from $[Fe(CN)_4NO]^{2-}$ in order to be subsequently released. We infer that this may occur under physiological conditions, with local situations (viz., near positively charged centers in membranes) favoring complex decomposition through the donor interactions of bound cyanides *(6)*.

The upper part of Figure 5 involves a set of reactions comprising the decomposition of I_1, occurring at a similar rate as its formation. The rigorous 2:1 stoichiometry in SNP/N_2O supports the disproportionation reaction described by Equations (21–22):

$$\left[Fe(CN)_4(NO)_2\right]^{2-} + CN^- + H^+ \rightarrow \left[Fe(CN)_5NO\right]^{2-} + HNO \quad (21)$$

$$2HNO \rightarrow N_2O + H_2O \quad (22)$$

Figure 2 includes an additional, parallel route for the decomposition of I_1, as revealed by the distinctive EPR signature of the final product at pH 5. We proposed it to be also a dinitrosyl species, $[Fe(CN)_2(NO)_2]$ (I_2), a new member of the well-characterized series of paramagnetic distorted tetrahedral complexes with different L ligands, described as $\{Fe(NO)_2\}^9$. These species behave as reversible, labile NO carriers, involved in *trans*-nitrosylation processes. EPR signals assignable to these dinitrosyl complexes have been found in tissue of ascite tumors of mice upon injection with SNP. Those containing L = thiolates and imidazole were found to activate sGC promoting vasodilation *(140)*.

Besides the mechanistic significance of the above results for understanding the SNP chemistry in biological fluids, an additional connection emerges with the still controversial mechanism of sGC activation *(141)*. The consensus is that smooth muscle relaxation is rapidly induced by low levels of NO. The fast response (within milliseconds) occurs because sGC efficiently binds to and is activated by NO. With the purified protein, NO-binding to the heme generates a 6C intermediate at a diffusion-controlled rate, which rapidly evolves to a 5C sGC-NO complex in which the bond between the heme iron and histidine has been broken, producing the crucial event for activation of the GTP → cGMP + pyrophosphate pathway. However, the kinetic evidence *(142,143)* suggests that the mechanism of the activation process is more complex: the 6C → 5C conversion involves an additional slower reaction that is of second-order in [NO], with $k = 2.4 \times 10^5\ M^{-1}\ s^{-1}$ at 4 °C *(142)*. It has been proposed that the second NO would occupy the proximal site, concomitant with the displacement of the histidine molecule, playing the role of a catalyst. It is not consumed in the process of generation

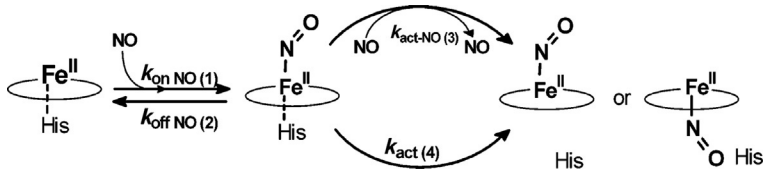

Figure 6 Proposed mechanism for the activation of sGC.

of 5C sGC-NO, which appears as necessary for full activation. This seems consistent with the formation of a low-activity complex with stoichiometric amounts of NO, whereas a high-activity complex is formed in excess NO *(142,143)*. Though the detailed mechanisms have not been clarified yet (*in vivo* and *in vitro* results differ significantly), the participation of dinitrosyls has been suggested as plausible *(141,144)*, based on a detailed study dealing with the behavior of another histidine-ligated heme protein, bacterial cytochrome *c′(144)*, which was found to display an analog behavior as sGC (cf. Figure 6). From our side, the previous analysis (Section 3.3.2) on the formation of *trans*-$[Fe(CN)_4(NO)_2]$ and $[Fe(por)(NO)_2]$, and particularly the subsequent reactivity leading to N_2O and $Fe^{II}(NO^+)$, allows suggesting that disproportionation of the *trans*-dinitrosyl species could lead to bound NO^- and NO^+ (or probably NO_2^-, depending on the pH). The NO^- could promote an even stronger *trans*-effect than NO (see below), in agreement with the found conversion of the proposed dinitrosyl to a final 5C complex with NO bound in the *proximal* heme pocket *(143)*.

3.4. Nucleophilic reactivity: The reactions of $[ML_5(NO)]^n$ with oxygen

In contrast with the $n=6$ systems, a nucleophilic reactivity might be anticipated for the more electron-rich metallonitrosyls. Although nitrosyl protonation reactions seem not to occur at the $\{MNO\}^7$ moieties (there are at most reports on hydrogen bonds being established with distal histidines, Ref. *(45)*), the reaction of $Mb^{II}NO$ with O_2 showed the formation of NO_3^- *(145)*. The decay of $[Fe(CN)_5(NO)]^{3-}$ upon consecutive additions of dissolved O_2 corresponds to the following stoichiometry:

$$4\left[Fe(CN)_5NO\right]^{3-} + O_2 + 2H_2O \rightleftarrows 4\left[Fe(CN)_5NO\right]^{2-} + 4OH^- \quad (23)$$

In excess of dissolved O_2, the concentration of $[Fe(CN)_5NO]^{3-}$ decays exponentially with a pseudo-first-order rate constant k_{obs} that correlates

linearly with $[O_2]$. This leads to a global second-order rate law: $-1/4\mathrm{d}[Fe(CN)_5NO^{3-}]/\mathrm{d}t = k_{23}[Fe(CN)_5NO^{3-}][O_2]$, with $k_{23} = (3.5 \pm 0.2) \times 10^5\ M^{-1}\ s^{-1}$ at 25 °C, pH 10 *(146)*. An excess of free CN^- was used to minimize *trans*-labilization of this ligand (Equation 16). The rate constant was insensitive to changes in pH (9–11) and ionic strength (0.1–1 M). An associative route has been proposed for the initial steps:

$$\left[Fe^{II}(CN)_5NO\right]^{3-} + O_2 \rightleftarrows \left[Fe^{III}(CN)_5N(O)O_2\right]^{3-} \quad k_{ad}, k_{-ad} \qquad (24)$$

$$\left[Fe^{III}(CN)_5N(O)O_2\right]^{3-} + \left[Fe(CN)_5NO\right]^{3-} \rightleftarrows 2\left[Fe(CN)_5NO_2\right]^{3-} \qquad (25)$$

In reaction (24), a new covalent bond forms between bound NO and O_2. The product is, according to DFT computations, a peroxynitrite anion bound to Fe(III); the anion has been also proposed as an initial intermediate in the reaction of $Mb^{II}NO$ with O_2 that subsequently isomerizes to NO_3^- as a final product *(145)*. Instead, we proposed the fast bimolecular formation of $[Fe(CN)_5NO_2]^{3-}$, Equation (25), with a subsequent reaction (26):

$$\left[Fe(CN)_5NO_2\right]^{3-} + \left[Fe(CN)_5NO\right]^{3-} + H_2O \rightleftarrows 2\left[Fe(CN)_5NO\right]^{2-} + 2OH^- \qquad (26)$$

The oxidation equivalents remain bound to the metal all along the reaction, leading to the experimentally found 4:1 global stoichiometry, without other detectable by-products. Under steady-state conditions for $[Fe^{III}(CN)_5N(O)O_2]^{3-}$, we get $-\mathrm{d}[Fe(CN)_5NO^{3-}]/\mathrm{d}t = 4k_{ad}k_{24}[O_2][Fe(CN)_5NO^{3-}]^2/(k_{-ad} + k_{24}[Fe(CN)_5NO^{3-}])$, which reduces to the observed rate law, with $k_{23} = k_{ad}$, when $k_{24}[Fe(CN)_5NO^{3-}] >> k_{-ad}$.

Second-order rate laws were also found for $[Ru(bpy)(tpm)NO]^{2+}$ *(30)* and $[Ru(NH_3)_5NO]^{2+}$ *(147)* complexes reacting with O_2. As the spin density distribution along the different $\{MNO\}^7$ moieties remains essentially invariable *(124)*, we expect similar reactivity patterns for the NO-complexes. The $[Fe(CN)_5NO]^{3-}$ and $[Ru(NH_3)_5NO]^{2+}$ complexes (affording $E_{NO+/NO}$ values at ~ -0.10 V) react with very similar addition rate constants, though the $[Ru(bpy)(tpm)NO]^{2+}$ ion ($E_{NO+/NO} = 0.55$ V) showed a much lower value of k_{ad}, by 5 orders of magnitude. Figure 7 shows a plot of ln k_{ad} against $E_{NO+/NO}$ for the three nonheme complexes. A linear trend can be appreciated, with a negative slope of $18.4 \pm 0.9\ V^{-1}$, in close agreement with a Marcus-type behavior. The plot also includes an estimated value for $Mb^{II}NO$. The mechanistic interpretation for the reaction of $Mb^{II}NO$ with O_2 is controversial; the observed rate constant has been

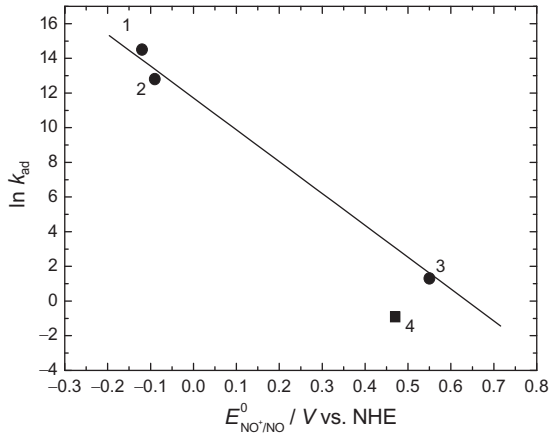

Figure 7 Plot of ln k_{ad} versus $E_{NO+/NO}$ for the reactions of O_2 with: (1) $[Ru^{II}(NH_3)_5NO]^{2+}$, (2) $[Fe^{II}(CN)_5NO]^{3-}$, (3) $[Ru^{II}(bpy)(tpm)NO]^{2+}$, and (4) $Mb^{II}NO$. See text for details on the latter species.

alternatively linked either to a step similar to reaction 24 or to the dissociation of NO from $Mb^{II}NO$ occurring as the rate-determining step, followed by O_2 binding at Mb^{II} and further attack by NO *(145)*. There is also some ambiguity in the redox potential for the $Mb^{III,II}NO$ redox couple, which was estimated through a thermodynamic cycle *(102)*.

Remarkably, the oxidation rate (reaction 23) decreased markedly at pHs <10 in the absence of cyanide, suggesting the unreactivity of $[Fe(CN)_4NO]^{2-}$ *(146)*. That 6C is a necessary condition to achieve autoxidation of bound NO-complexes agrees with a similar reactivity pattern found in nonaqueous media for the nonheme $[Fe(PaPy_3)NO]^+$ complex *(21)*. Also, the picket-fence compound [Fe(TpivPP)NO] (TpivPP = α,α,α,α,-tetrakis (*o*-pivalamidophenyl)-porphyrin dianion) reacts with O_2 *only* in the presence of pyridine, to give $[Fe(TpivPP)(NO_2)(py)]$ *(148)*. The increase in O_2-reactivity when going from 5C to 6C nitrosyls is consistent with the increase in the radical character of the NO group, as discussed above. Finally, that the redox potentials of the $M–NO^+/M–NO^\bullet$ couples could predict the NO-autoxidation reactivities appears as quite significant. Some $NO^\bullet$-coordination compounds could readily react with O_2 in order to provide a fast route to $NO^\bullet$-consumption. However, the complexes like $[Fe(CN)_5NO]^{3-}$ could hardly compete with other main sinks for NO, namely its very fast reactions with sGC or with HbO_2. On the other hand, we turn back to sGC, searching for the mechanism of enzyme recovery of catalytic activity, i.e., the back conversion of sGC-NO to sGC. Given the low values of k_{off}

for NO-release from 5C sGC-NO ($\sim 10^{-3}$–10^{-4} s^{-1}) *(73,74,141)*, the 6C requirement for O_2-attack to the 5C sGC-NO in the plentiful oxygen medium could be important, linked to histidine rebinding, NO-release from the labile "NO-ferric heme," and further Fe(III) reduction by NO.

4. COMPLEXES WITH $n = 8$

4.1. Structure, spectroscopy, and electronic description: Dominant $^1NO^-/^1HNO$ ($S = 0$)

Species with $\{M–NO\}^8$ configuration have been reached by reduction of the corresponding $\{M–NO\}^{6,7}$ either chemically or electrochemically. The CV experiments performed on $\{M–NO\}^6$ compounds usually show two 1-electron reduction waves in aqueous solutions. The first one shows up in the range −0.4 to +0.6 V, depending on the MX_5 fragment. The second reduction wave, most frequently irreversible, occurs at ~0.8–1.0 V more negative potentials *(149)*. Free NO^- (a species that is isoelectronic with molecular oxygen) has a triplet GS. Coordination to a metal center splits the degeneracy of the π^*_{NO} orbitals, and consequently, the GS of $\{M–NO\}^8$ coordination compounds of d^6 metal centers has always been described as singlet in character *(16,17)*.

As with $n = 7$, both 5C and 6C compounds can be achieved, though an even stronger *trans*-effect must be expected as a result of the increased population of the $\pi^*_{NO(\sigma)}$ orbital. Compared to the species in the higher oxidation states of coordinated NO, M–(NO^-) complexes are more electron-rich, a situation that might eventually lead to protonation at the nitrogen lone pair, yielding complexes with coordinated HNO. Table 3 displays a selected number of well-characterized 5C or 6C species, with available X-ray structural data or reliable combined spectral/computational information, containing either bound NO^- or HNO.

4.1.1 NO^--complexes

The X-ray structure of a 5C Co(III)-(TPP) complex was described for the first time in 1973 *(160)*, though a higher quality crystal structure determination was reported later *(152)*. This species was obtained by reaction of the corresponding Co(II)-(TPP) with NO, and it is a representative example of a number of well-defined Co(III)-(NO^-) porphyrinate systems, which are all diamagnetic and square-pyramidal *(18,53)*, as is also the recently prepared Co(III)-LN_4 complex with four asymmetrically bound basal N-ligands in a nonmacrocyclic heme platform *(161)*. The Co(III)-tropocoronand

Table 3 Selected list of 5C and 6C nonheme- and heme-nitrosyl complexes, $[MNO]^8$ (M = Co, Fe, Ru, Os, Ir)[a]

		Compound	ν_{NO} (cm^{-1})	d_{M-N} (Å)	d_{N-O} (Å)	$\angle_{MNO}$ (deg)	Ref.
NO^-	6C	$[Co(en)_2Cl(NO)]ClO_4$	1611	1.820(11)	1.043(17)	124.4(11)	*(150)*
		$NOCbl{\cdot}15H_2O$	–	1.927(6)	1.14–1.20	121–117	*(151)*
		Fe(cyclam-ac)(NO)[b]	1271	1.752	1.261	122.4	*(24)*
		$[Ru(Me_3[9]aneN_3)(bpy)NO]^+$	1315, 1286 1404[b]	1.91	1.27	122.9	*(15)*
NO^-	5C	Co(TPP)(NO) (sqp)	1681	1.8301(5)	1.1492(7)	~123.39(5)	*(152)*
		Co(TCC-4,4)(NO) (tbp)	1584	1.779(6)	1.151(9)	128.9(6)	*(153)*
		Co(TCC-3,3)(NO) (sp)	1656	1.785(6)	1.137(7)	127.3(6)	*(153)*
		$Co(LN_4)(NO)$ (sp)	–	1.7890(11)	1.1551(15)	125.97(9)	*(154)*
		$[Fe(CN)_4(NO)]^{3-}$ (tbp)[b]	1581	1.637	1.22	171.2	9
		$[Fe(TFPBr_8)(NO)]^-$ (sp)[b]	1547	1.790	1.201	122.7	*(155)*
HNO	6C	$[Fe(cyclam\text{-}ac)(HNO)]^+$[b]	1351	1.78	1.27	126.3	*(24)*
		$Mb^{II}(HNO)$[c]	1385	1.82	1.24	131	*(156)*
		$[Fe(CN)_5(HNO)]^{3-}$[b]	1338, 1394	1.783	1.249	137.5	*(12)*
		$Ru(py^{bu}S_4')(HNO)$	1358	1.875(7)	1.242(9)	130.0(6)	*(157)*
		$[Ru(Me_3[9]aneN_3)(bpy)(HNO)]^{2+}$[b]	1376	1.93	1.28	127.5	*(15)*
		$[Os(Cl)_2CO(PR_3)(HNO)]$	1410	1.915(6)	1.193(7)	136.9(6)	*(158)*
		cis–trans-$IrHCl_2(PPh_3)_2(HNO)$	1493	1.879(7)	–	129.8(7)	*(159)*

[a]Total spin $S = 0$, unless otherwise indicated. Nitrosyl stretching frequencies (ν_{NO}) and relevant distances and angles have been detailed.
[b]From DFT.
[c]From XAFS.
Abbreviations: en = ethylenediamine; LN_4 = diimine/dipyrrolide dianion; Mb = myoglobin; NOCbl = nitrosylcobalamin; PR_3 = trialkylphosphine; '$py^{bu}S_4$' = 2,6-bis-(2-mercapto,3,5-di-*t*-buthyl-phenylthiomethyl)pyridine dianion; TC-3,3 = tropocoronand 3,3; TC-4,4 = tropocoronand 4,4; $TFPBr_8$ = 2,3,7,8,12,13,17, 18-octabromo-5,10,15,20-[tetrakis-(pentafluorophenyl)]porphyrin dianion. See Tables 1 and 2 for other abbreviations.

(TCC) derivatives show a distinctive behavior: the diamagnetic 4,4-complex shows a bent nitrosyl in the equatorial position of a trigonal bypyramid, while the 3,3-complex is a paramagnetic square-pyramid *(153)*.

A series of 5C Fe-nitroxyl heme-complexes have been obtained by reducing the corresponding $n=7$ compounds with cobaltocene derivatives in nonaqueous medium *(154,161)*. The diamagnetic $TFPBr_8$-compound (Table 3) has been isolated and characterized by UV–vis, FTIR, ^{1}H,^{15}N NMR spectroscopies and DFT calculations and is very stable in CH_2Cl_2, in the absence of oxygen *(155)*. The electronic structure of the latter has been described as intermediate between $Fe^{II}NO^{-}$ and $Fe^{I}NO$, in agreement with computations in the 6C $[Fe(por)(MI)(NO)]^{-}$ *(162)*. The enhanced stability compared to other unstable 5C TPP- and OEP-nitroxyls can be traced to the electron-withdrawing groups in the porphyrin ring which also induce a positively shifted reduction potential for the $n=7$ complex. In a related way, the $[Fe(3,5\text{-Me-BAFP})(NO)]^{-}$ ion has been characterized as a result of spectroelectrochemical reduction of the $n=7$ compound (Table 2) *(116)*. Table 3 also includes the calculated DFT structural parameters for the $[Fe(CN)_4(NO)]^{3-}$ complex, which is presumably generated as a moderately stable species upon cyanide-labilization from the unstable $[Fe(CN)_5(NO)]^{4-}$ ion (see below) *(12)*.

Back in 1970, $[Co(en)_2Cl(NO)]ClO_4$ was prepared by reacting a Co(II) precursor with NO *(150)*, yielding the first X-ray structure of a 6C complex. A similar strategy led to $[Co(NH_3)_5(NO)]Cl_2$. Both complexes show enhanced distances for Co(III) and the *trans*-ligands (Cl^{-}, NH_3), by ~0.3 Å *(150)*. Other analogs with Schiff bases, dithiocarbamates, dimethylglyoximates, and other chelating coligands have been prepared *(150)*. Most significant was the isolation in 2007 of nitroxylcobal(III)amin (NOCbl, containing a corrin ring), obtained by reaction of hydroxycobalamine·HCl with a NONOate *(151)*. The Co–N_α axial bond length to the DMB ligand of NOCbl is greater by 0.13 Å than the distance in the related NO_2Cbl structure, reflecting the *trans*-labilizing effect of NO^{-}. Both the axial "base-off" and "base-on" complexes coexist in aqueous solution at mild acidities, with predominance of the latter (deprotonated) form at pHs ≥7 *(163)*. In an important application of the properties of Co(II)(por)/Co(III)(por) fragments toward nitrosyl/nitroxyl coordination, a novel amperometric method has been developed, based on the attachment of a Co(II)(por) to a gold electrode and further electrochemical oxidation to Co(III). The latter species can selectively bind HNO over NO upon the exposure to HNO/NO donors *(164)*. Though not included in Table 3,

it is worth mentioning that NO^--complexes have been also prepared with Rh(III) and Pt(IV) low-spin d^6 metal centers *(165)*.

The first 6C Fe^{II}-nitroxyl complex, *trans*-[Fe(cyclam-ac)(NO)], has been thoroughly characterized in acetonitrile solution by reducing chemically or electrochemically the $n=7$ complex *(24)*. The calculated metric data show the Fe–N, N–O distances and FeNO angle (close to 120°) at similar values than for the 5C Fe(II) heme-complex, though υ_{NO} is significantly lower, suggesting the O-donor ability of the acetate ligand *trans* to nitroxyl. The structure was described as $Fe^{II}NO^-$. Remarkably again, the calculated Fe–O distance is 0.14 Å longer than in the $n=7$ analog (and 0.26 Å longer than for the $n=6$ one), reflecting the *trans*-effect of NO^-. While the chelating ligand avoids the release of the acetate arm in acetonitrile solution, the closely related complex *trans*-[Fe(cyclam)Cl(NO)] did not maintain its integrity under the same conditions after reducing the $n=7$ derivative (Table 3), presumably because of the exchange of the chloride ligand with the solvent or reoxidation to the starting material *(111)*.

A Ru^{II}-(NO^-) complex could be well characterized by electrochemical reduction of the $n=7$ $[Ru(Me_3[9]aneN_3)(bpy)(NO)]^{2+}$ complex at −0.23 V, in acetonitrile *(15)*. As with [Fe(cyclam-ac)(NO)] *(24)*, the reduction process can be represented by Equation (27):

$$[Ru(Me_3[9]aneN_3)(bpy)(NO)]^{2+} + e^- \rightarrow [Ru(Me_3[9]aneN_3)(bpy)(NO)]^{+} \quad (27)$$

The $\{Ru\text{-}NO\}^8$ species displays a υ_{NO} that is ∼300 cm^{-1} lower (cf. Table 3) than the value measured in the $n=7$ precursor, in agreement with other reports (cf. Table 2). The electronic spectrum showed a typical pattern of bands, which were adequately reproduced by the (TD) DFT analysis. Interestingly, the aqueous spectroelectrochemical preparation at pH 12.8 also led to a product with similar electronic absorptions as in acetonitrile, suggesting the formation of the same species than in water. The NO^--complex showed to be remarkably stable in both aqueous- and acetonitrile media, in the absence of oxygen. The metric data provided by DFT computations are quite consistent with those calculated for [Fe(cyclam-ac)(NO)] *(24)*.

4.1.2 HNO-complexes

The intermediacy of HNO-complexes in redox, metal-bound NO/NH_2OH conversions was early suggested by Roper's work in 1970 *(166)*

and led in 1979 to the first crystal structure of an HNO-complex, $[Os(Cl)_2(CO)(HNO)(PPh_3)_2]$ *(158)* (Table 3). Though only two (Ru- and Ir-) additional compounds with X-ray crystal structures are available, a greater number of well-characterized compounds have been described *(16,17,70,71,167)*. Different synthetic strategies have been used for preparing nonheme and heme HNO-complexes (also containing Fe and Re metals) *(16,17)*. In short, the procedures have involved using either specific oxidation pathways (viz., $Pb(OAc)_4$ with a Re-bound hydroxylamine-precursor in CH_2Cl_2*(168)*), or differently elaborated reductions of NO^+- or NO-complexes by using 2-electron reductants like hydrides *(157)*, or 1-electron reductants, including electrochemical techniques. Recently, bulk electrolysis in THF of a bis-picket-fenced iron-porphyrin, [Fe(3,5-Me-BAFP)] (Table 2), led to a heme-based 1-electron reduction. Addition of NO led to the nitroxyl (NO^-) derivative, which in turn was treated with acetic acid to yield [Fe(3,5-Me-BAFP)(HNO)], the first ferrous heme-HNO model complex *(116)*. The latter has an electronic spectrum that resembles Farmer's Mb(II)-HNO complex *(156)*.

We succeeded in the preparation of $[Fe^{II}(CN)_5HNO]^{3-}$ in aqueous anaerobic solution by reaction of SNP with 2 equiv. of dithionite at pH 10 in the presence of an excess of free cyanide (Figure 8) *(13)*. The reduction led to nearly quantitative formation of the product as revealed spectrophotometrically. Using BH_4^- as an alternative reductant has been recommended as a better choice for preparing $[Fe^{II}(CN)_5HNO]^{3-}$, though only ~20% yields could be reached *(169)*. The main absorption band of

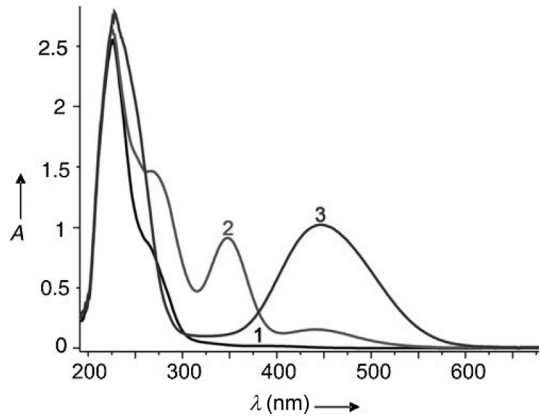

Figure 8 Spectra of $[Fe(CN)_5(NO)]^{2-}$ (1) and the one- and two-electron reduced complexes $[Fe(CN)_5(NO)]^{3-}$ (2) and $[Fe(CN)_5(L)]^{n-}$ (3) (L = HNO,NO^-) obtained by two sequential 1 equiv. additions of $S_2O_4^{2-}$ to 3×10^{-4} M at pH 10, $T = 25.0$ °C.

the $[Fe^{II}(CN)_5HNO]^{3-}$ anion at 445 nm showed to be fairly persistent at pH 10, reverting to $[Fe(CN)_5NO]^{3-}$ (high yield, >80%), with a half-life time of ~50 min. However, and rather surprisingly, a rapid shift to pH ~6 immediately after completing the 2-electron reduction allowed attaining a great stability of the 445 nm band intensity, which decayed with a pseudo-first-order rate constant of $\sim 10^{-6}$ s^{-1} *(14)*. The metric data (Table 3, previously obtained employing DFT) and the ATR/FTIR evidence were in agreement with an HNO-bound species, in full consistency with the crucial ^{1}H-NMR experiment showing δ at 20.02 ppm and J_{NH} at 71.14 Hz (pH 6). NMR measurements have been determinant for the early unambiguous identification of HNO in the Os(II)-, Re(I)-, and other complexes. RR results (with ^{14}N- and ^{15}N-labeled NO), obtained after irradiation close to the 445-nm band, showed the disappearance of bands characteristic of $[Fe(CN)_5NO]^{2-}$ upon reduction, along with typical new absorptions assigned to $[Fe(CN)_5HNO]^{3-}$ (υ_{NO} at 1380 cm^{-1}), consistent with the IR results.

Importantly, the $[Ru(Me_3[9]aneN_3)(bpy)(HNO)]^{2+}$ ion could be generated in aqueous solution by electrochemical reduction of $[Ru(Me_3[9]aneN_3)(bpy)(NO)]^{2+}$ at pH 2.5 *(15)*. Though the electrochemical wave at ~−0.3 V showed irreversible in the CV time scale, a controlled potential coulometry led reversibly to a stable product with an electronic spectrum very different from the one obtained at pH = 12.8 or in acetonitrile. The half-wave potential of the couple correlated with the pH with a slope of 60 mV per pH unit, suggesting a proton-coupled 1-electron reduction (Equation 28).

$$[Ru(Me_3[9]aneN_3)(bpy)(NO)]^{2+} + e^- + H^+ \rightarrow [Ru(Me_3[9]aneN_3)(bpy)(HNO)]^{2+} \quad (28)$$

For a given metal fragment, the metric data for the HNO- and NO^--complexes are similar, reflecting a double-bond N–O character in both cases. On the other hand, the angles in the NO^--complexes approach the limit of 120° more than the HNO-complexes do, suggesting the influence of greater repulsion effects of the lone-pairs at the N-atom. As shown by recent calculations *(170)*, the M(II)-complexes (viz., $[M^{II}(por)(5\text{-MeIm})(HNO)]$, M = Fe, Ru) show significantly smaller values of υ_{NO} (1399–1376 cm^{-1}) than $[M^{III}(por)(5\text{-MeIm})(HNO)]^+$ (M = Co, Rh, Ir), at ~1500 cm^{-1}, probably because of a greater back-donation. These trends are confirmed by the data for complexes in Table 3.

The 6C HNO-complexes show similar *trans*-L distances to the ones observed in related complexes that contain a weak-to-moderate π-acceptor ligand, like the NO_2^- group *(15)*, suggesting the lack of *trans*-labilization effect. This is in contrast with the elongations shown by the NO^--related derivatives. The result is illuminating for the analysis of the comparative activation roles of NO, NO^-, or HNO for sGC. By performing experiments with non-native sGC prepared by substituting the hemin of the native enzyme with Mn^{II}(PPIX) and Co^{II}(PPIX) (PPIX = Protoporphyrin IX), addition of NO revealed the activation trend: sGC(Co) > sGC(Fe) ≫ sGC (Mn), which correlates with $n = 8(Co^{III}) > n = 7(Fe^{II}) \gg n = 6(Mn^{II})$ *(171)*. The role of HNO on the activation of sGC has been controversial *(169)*; recent theoretical calculations *(172)* suggest that no activation should be feasible, supporting the presently reported results and reflecting the profound electronic influence of protonation of the NO^- ligand.

4.2. Characterization of the NO^-/HNO interconversions in solution

Most of the preparative work on the $n = 8$ complexes has been carried out in nonaqueous solvents, and only some hints on the chemistry of the relevant species are available in these media *(16,17)*. A serious drawback is the dominant insolubility of most of the reported compounds in water, as well as the scarce iron-containing examples. In the following, we will focus on the above discussed $n = 8$ Fe- and Ru-complexes. The different metal–coligand framework allowed assessing a quite different chemical behavior in water solution.

Once the characterization of $[Fe(CN)_5HNO]^{3-}$ at pH 6 was conclusive, we afforded an NMR titration experiment with OH^-, searching for deprotonation. The integrated intensity of a signal at 20.02 ppm decays with increasing pH *(13)*. This signal disappears at pH 10 and is partly recovered when the pH is returned to 6–7. By assuming reaction (29), we estimated $pK_a = 7.7$:

$$\left[Fe(CN)_5HNO\right]^{3-} \rightleftarrows \left[Fe(CN)_5NO\right]^{4-} + H^+ \quad K_a \tag{29}$$

The value of 7.7 was reported as a first estimation of the acidity of bound-^{1}HNO in coordination compounds. It seemed a reasonable value, given that the pK_a of the free $^1HNO/^1NO^-$ conversion has been estimated at ~23 *(173)*. However, some ambiguity was apparent from the fact that the band maximum in the electronic spectrum of the titration product at

pH 10 was essentially identical to the one at pH 6. This seems inconsistent, given that the 445-nm band (MLCT in origin) should expectedly shift upon deprotonation of HNO. Besides, the properties of the stable iron heme-nitroxyl derivative $Hb^{II}HNO$ (Table 3) were reported to remain unchanged in aqueous solution up to pH ~10–11 *(17,169)*.

At the time we reported the pK_a for $[Fe(CN)_5HNO]^{3-}$, we had payed no much attention to our own previous computational DFT result predicting that $[Fe(CN)_5NO]^{4-}$ was an *unstable* species that should lose CN^- from the coordination sphere, in contrast with the successful predictions on the stability of other 5C and 6C cyano-nitrosyl complexes *(12)*. Anyway, we considered a plausible decomposition route for the putative $[Fe(CN)_5NO]^{4-}$ intermediate, involving the *trans*-labilization of cyanide (Equation 30):

$$\left[Fe(CN)_5NO\right]^{4-} \rightleftarrows \left[Fe(CN)_4NO\right]^{3-} + CN^- \quad K_{trans} \tag{30}$$

This reaction type has been thoroughly explored for $[Fe(CN)_5NO]^{3-}$ ($n=7$) in reaction (16), with pK_{16} ~4, and leads to a dominant yield of the blue $[Fe(CN)_4NO]^{2-}$ species that is predominant even in neutral solution because of the protonation of free cyanide *(134)*. In this context, we trusted that reaction (30) could be reverted to the left at pH 10 by adding an excess of free cyanide to the solutions. Some experimental evidence points to the electrochemical generation of aqueous $[Fe(CN)_4NO]^{3-}$ *(174)*. In the electronic spectrum of the solutions of $[Fe(CN)_5HNO]^{3-}$ employed for the experiments, we also detected an asymmetry of the main absorption band at 445 nm, supporting the presence of an absorption which could well be due to $[Fe(CN)_4NO]^{3-}$. Eventually, a calculated electronic spectrum of the latter showed weak absorption bands in the 500–600 nm range. Interestingly, the theoretical work predicts bipyramidal geometry for the latter anion, with the nitroxyl in the equatorial position *(12)*.

In the meantime, our work with $[Ru(Me_3[9]aneN_3)(bpy)(HNO)]^{2+}$, on which we expand below, led to a reliable value of $pK_a = 9.8$ for bound HNO *(15)*. Though not only the metal center but also the coligands are dissimilar compared to $[Fe(CN)_5HNO]^{3-}$, we are reelaborating on the real significance of 7.7 as the midpoint of the titration curve in Figure 9. As a preliminarily modified approach, we believe that the value of 7.7 might be an apparent pK that results from the coupling of reactions (29) and (30). Therefore, the measured value would be the sum of pK_{29} and pK_{30}.

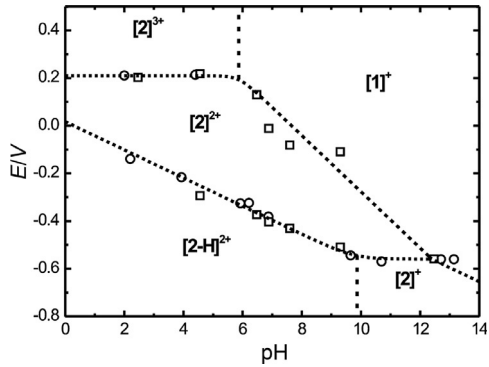

Figure 9 Potential (E°)–pH diagram showing the redox and acid–base behavior of the system based on the $[Ru(Me_3[9]aneN_3)(bpy)]^{n+}$ fragment. **[1]**$^{+}$ = $[Ru(Me_3[9]aneN_3)(NO_2)]^{+}$; **[2]**$^{n+}$ = $[Ru(Me_3[9]aneN_3)(NO)]^{n+}$ ($n = 1, 2, 3$); **[2-H]**$^{2+}$ = $[Ru(Me_3[9]aneN_3)(HNO)]^{2+}$. Data arising from CV and SWV experiments are displayed as squares, while those originating from spectroelectrochemistry are represented as circles.

By *assuming* that pK_{29} (pK_a) is ~10, we obtain a value of −2.3 for pK_{30}. Given that for the $\{FeNO\}^7$ holding species pK_{16} ~4, it results that the equilibrium constant for the cyanide-labilization reaction is ~6 orders of magnitude greater for $[Fe(CN)_5NO]^{4-}$ than for $[Fe(CN)_5NO]^{3-}$, which seems consistent with the previous analysis of comparative *trans*-effects of NO^- and NO. In this new context, it results that the transient $[Fe(CN)_5NO]^{4-}$ species should remain in a negligible steady-state concentration during the NMR titration. Even though equilibrium *(28)* might not evolve to completion in the underlying conditions, the main product $[Fe(CN)_4NO]^{3-}$ can revert to $[Fe(CN)_5HNO]^{3-}$ in a high yield by reacidification in the minute time scale according to reactions (29) and (30). In a longer time scale, the slow redox conversion giving $[Fe(CN)_5NO]^{3-}$ (345 nm) reveals an alternative oxidative decay of $[Fe(CN)_4NO]^{3-}$, probably through solvent reduction, or through an unknown disproportionation path *(13)*. A very recent work *(175)* reinforces the proposal of a pK_a >10, on the basis of reported ^{17}O NMR measurements with the isotopically labeled $[Fe(CN)_5HN^{17}O]^{3-}$ at different pH-values, revealing the conservation of the main ^{17}O signal in the pH range 6–10. In this work, the loss of the ^1H NMR signal in the range 7–10 is ascribed to a fast acid–base catalyzed hydrogen exchange and not to the actual speciation. These arguments are still unable to account for the different chemical properties of the corresponding solutions at pH 6 and 10, as discussed below.

We tried to surpass the ambiguities with the pentacyano-nitroxyl system by designing a new Ru-complex, as anticipated above, with the following issues in mind: (i) the Ru-complexes ought to be more inert toward ligand exchange processes than the Fe-analogs. (ii) The use of chelating ligands, as successfully exemplified by the use of a pendant-acetate arm cyclam-ac, would prevent the exchange of the ligand *trans* to nitroxyl *(24)*. (iii) The new complex should be soluble in both solvents, acetonitrile and water, in order to go a step further in the comparisons with the reported chemistry of [Fe(cyclam-ac)(NO)]. Inspired in already classic synthetic strategies, we isolated a salt of the $[Ru(Me_3[9]aneN_3)(bpy)(NO_2)]^+$ ion by reacting the aqua-precursor with nitrite, followed by the conversion of the nitro-complex to the $[Ru(Me_3[9]aneN_3)(bpy)(NO)]^{3+}$ ion (cf. Equation 1). Both complexes were characterized by X-ray diffraction, NMR, IR, and UV–vis spectroscopies, cyclic voltammetry (CV), UV–vis/IR spectroelectrochemistry, and theoretical calculations (DFT, (TD)/DFT). Spectroelectrochemical reductions in acetonitrile and aqueous solutions allowed identifying the $n=7$ and $n=8$ species, as well as the acid–base interconversion between bound HNO and NO^-. We focus on the latter issue and drive the reader to Tables 1–3 in order to compare the metric data for the three nitrosyl redox states, which allowed establishing well-defined trends in the distances, angles, IR-results, *trans*-effects, and back-bonding abilities.

4.3. A potential-pH diagram in aqueous solution for the different complexes based on the $[Ru(Me_3[9]aneN_3)(bpy)]^{2+}$ fragment

Figure 9 resumes a thermodynamic picture for the predominance of five nitrogenated species with bound NO^+, NO, NO^-, HNO, and NO_2^-, under variable pH and redox potential conditions. The diagram was build up from the combination of CV, square-wave voltammetry (SWV), and spectroelectrochemical experiments. The different regions of thermodynamic stability for the $\{RuNO\}^n$ species are clearly defined. The line that separates the $n=7$ from $n=8$ compounds breaks at a pH close to 10, due to reaction (31).

$$[Ru(Me_3[9]aneN_3)(bpy)(HNO)]^{2+} \rightleftarrows [Ru(Me_3[9]aneN_3)(bpy)(NO)]^{+} + H^+ \quad (31)$$

A complementary acid–base titration and global analysis of the UV–vis spectra allowed measuring values of $pK_a = 9.78 \pm 0.15$ for reaction (31). The reader might access to the details in the published article *(15)*.

As a preliminary conclusion on the measurements of pK_a for bound HNO in aqueous solutions, we might consider that a value of ~10 is most reliable, probably with some dependence on the metal center and the more so with eventual variation of the coligands. Further work is needed for clarifying these important issues, with a desirable extension to the heme-systems. In any case, the speciation of M–(HNO) or M–(NO^-) complexes appears to be not only dependent on the pK_a values. If this were the case, M–(HNO) species should be always highly predominant in neutral solutions, with no relevant participation of M–(NO^-). As discussed above, the coupled situation implying the *trans*-labilizing influence of NO^--complexes could facilitate the presence of the latter species even in neutral media.

4.4. Comparative reactivity of NO^- and HNO complexes

There are different reactivity modes that have been explored for the Fe- and Ru-complexes presented above.

4.4.1 Ligand exchange in solution

We must differentiate between the ability of NO^- and other coligands toward dissociation in solution. The most significant results reveal that the labilization of the coligand *trans* to NO^- is a general feature for the 6C complexes, as shown by $[Fe(CN)_5NO]^{4-}$ *(12)*, [Fe(cyclam)(Cl)(NO)] *(111)*, and NOCbl *(151,163)*. As $[Fe(CN)_4NO]^{3-}$ and CN^- revert to $[Fe(CN)_5HNO]^{3-}$ upon acidification to pH 6, the $[Fe(CN)_5NO]^{4-}$ ion apparently behaves as a true intermediate, i.e., the Fe-nitroxyl bond is conserved under the varying pH-conditions. The DFT calculations reveal a multiple Fe–NO bond character in the [Fe(cyclam-ac)(NO)] complex *(24)*; in this case, the stability also relates to the presence of the acetate-binding arm avoiding the *trans*-labilizing decomposition mode. The $[Ru(Me_3[9]aneN_3)(bpy)(NO)]^+$ complex behaves also as a robust system, suggesting a high contrast with the very labile $n=7$ complex, [Ru(cyclam)(Cl)(NO)] *(176)*. That the Fe–NO^- bond is very strong and negligibly dissociative has been also observed with the 5C Fe(TFPPBr$_8$)NO complex in nonaqueous medium *(155)*.

As for the HNO-complexes, all the available evidence in nonaqueous and aqueous media suggest that these species are inert with respect to HNO-dissociation (the *trans*-effect is negligible). A recent revision of the aqueous solution behavior of $[Fe(CN)_5HNO]^{3-}$ shows that its main absorption band at 445 nm decays very slowly at pH 6, through an oxidation process of HNO leading mainly to $[Fe(CN)_5NO]^{2-}$, with k_{decomp}

$\sim 5 \times 10^{-7}$ s^{-1} at 25 °C (negligible N_2O-formation) *(14)*. The latter value is a low limit to k_{-HNO}, the specific dissociation rate constant for HNO. By comparing with related $[Fe^{II}(CN)_5L]^{n-}$ complexes, the order of k_{-L}s is: $NO^+ \ll CO < CN^- < HNO < NOBz < NO < dmso < pz < py < NH_3$, with the latter k_{-NH3} at $\sim 10^{-2}$ s^{-1}. HNO fits in an intermediate position, reflecting its ubiquity in the so-called spectrochemical series, which reflects the capability of the L ligands toward σ–π bonding to iron *(14)*.

Finally, we go briefly on the coordination ability of free NO^-/HNO into metal centers containing a vacant or labile site. In general, mixing nitroxyl-donors with heme-M(III) complexes ($M = Fe^{III}$, Mn^{III}) leads to reductive nitrosylations, with formation of M^{II}–NO *(177)*. On the other hand, Fe(II) complexes like Mb^{II} allowed trapping HNO from the solutions containing the same donors, forming Hb^{II}–HNO, in competition with the fast dimerization of HNO to N_2O *(17)*.

4.4.2 Redox reactivity

There is a great difference between related NO^-- and HNO-analog complexes concerning their redox-chemistry. The HNO-derivatives appear as mild reductants, while the NO^- species behave as strong reductants. Quite revealing are the results for the reactions of the 2-electron reduction products of $[Fe(CN)_5NO]^{2-}$ at pH 6 and 10, with poorly oxidizing reagents. With methylviologen (MV^{2+}, $E^\circ = -0.44$ V), no reaction is observed at pH 6 with $[Fe(CN)_5HNO]^{3-}$. On the other hand, at pH 10, the reduced viologen radical can be immediately appreciated after mixing *(14)*. A similar result follows the addition of 1 equiv. of $[Fe(CN)_5NO]^{2-}$, a weak oxidant ($E^\circ = 0.05$ V), to the nitroxyl complexes. At pH 6, no spectral changes are apparent; however, at pH 10 the immediate formation of $[Fe(CN)_5NO]^{3-}$ is achieved, revealing quantitatively a comproportionation process, reaction (32), preceded by the reverse of reaction (30).

$$\left[Fe(CN)_5NO\right]^{4-} + \left[Fe(CN)_5NO\right]^{2-} \rightleftarrows 2\left[Fe(CN)_5NO\right]^{3-} \qquad (32)$$

The results suggest a value of $E^\circ \ll 0.4$ V for the cyano-NO^--complexes, while $[Fe(CN)_5HNO]^{3-}$ affords an estimated value of 0.3 V, in terms of the oxidation wave measured in the CV at pH 6 *(14)*, which has been assigned as corresponding to the proton-coupled redox potential, E° (FeNO, H^+/FeHNO). This is remarkable, because the related potential

for NO, H^+/HNO has been reported to be at −0.55 V at pH 7 *(16,17)*, suggesting that aqueous free HNO is a strong reductant.

In contrast with our observations, it has been stated that $Mb^{II}HNO$ reacts with MV^{2+} at pH 10, yielding MV^+ *(17)*. If the latter speciation is correct at that pH, the result is the opposite as expected, at least by comparing with $[Fe(CN)_5HNO]^{3-}$. As the real pK_a values for bound-HNO deprotonations seem to still need a closer scrutiny, the values of the redox-potentials for the bound NO^- and HNO-couples should be accordingly considered as subject to revision.

The $[Fe(CN)_5HNO]^{3-}$ ion reacts with $[Fe(CN)_6]^{3-}$ ($E^\circ \sim 0.4$ V), according to reaction (33):

$$\left[Fe(CN)_5HNO\right]^{3-} + 2\left[Fe(CN)_6\right]^{3-} \rightleftarrows \left[Fe(CN)_5NO\right]^{2-} + 2\left[Fe(CN)_6\right]^{4-} + H^+ \qquad (33)$$

The rate-law is first order in each reactant, with $k_{33} = 70\ M^{-1}\ s^{-1}$ at 25 °C *(14)*. This value is of the same order of magnitude as the one measured for free HNO reacting with $[Fe(CN)_6]^{3-}$ *(16)*. If we assume an initial slow 1-electron oxidation of $[Fe(CN)_5HNO]^{3-}$ by $[Fe(CN)_6]^{3-}$, followed by a rapid oxidation to $[Fe(CN)_5NO]^{2-}$, the use of the Marcus "cross-reaction" model to the first step led to a value of $6 \times 10^{-3}\ M^{-1}\ s^{-1}$ for the self-exchange rate constant for the $[Fe(CN)_5NO]^{3-}$,H^+/$[Fe(CN)_5HNO]^{3-}$ redox couple. This is a very low value compared to the much higher exchange-rates for the $[Fe^{II}(CN)_5L]^{n-}$ complexes ($\sim 10^5\ M^{-1}\ s^{-1}$), which react through metal-centered electron-transfers when L is nonredox active. On the other hand, reaction (33) appears to involve a ligand-centered redox reaction, involving a proton-coupled process with high reorganization energy *(91)*.

In the preliminary experiments of SNP reduction with dithionite, we verified that an excess of reductant over the necessary 2 equiv. for attaining bound HNO induced the decay of the 445-nm band. This was indicative of probable further reduction and led us to perform a kinetic study of the reaction of $[Fe(CN)_5HNO]^{3-}$ with dithionite at pH 6. In short, the stoichiometry and rate-law allowed establishing that a 4-electron reduction was operative, with NH_3 as a final product, suggesting the onset of consecutive ligand-centered processes with N-bound intermediates *(14)*. In fact, the overall 6-electron process starting from SNP down to $[Fe(CN)_5NH_3]^{3-}$ resembles the gross reactivity features of assimilatory nitrite-reductases *(46)*.

4.5. Nucleophilic reactivity: The reactions with dioxygen

A comprehensive set of 5C [$Co^{III}L_4(NO^-)$] complexes (L = quadridentate or bis-bidentate platforms) react with O_2 in nonaqueous media in the presence of nitrogen or phosphorus bases (B) to yield the corresponding 6C nitrocompounds, *trans*-[$Co(L_4)(B)(NO_2)$] *(178)*. The rates depend strongly on the nature of B, influencing the nucleophilicity of the $\{CoNO\}^8$ moieties. The mechanism has been described as an initial equilibrium of the 5C–6C species, with *only* the latter reacting with O_2 and leading to a $\{Co(L_4)(B)N(O)O_2\}$ peroxynitrito-intermediate in the rate-determining step. This step is followed by fast dimerization with another $\{CoL_4B(NO)\}$ unit, homolysis of the O–O bond, and final formation of the nitro-complex. Other Co-, Ru-, and Ir-complexes react similarly in the initial step, though with the formation of nitrato complexes as final products, presumably through the isomerization of the N-bound peroxynitrito-intermediate to the O-bound species *(179)*. The factors influencing one or other type of stoichiometry are not clearly understood. More recently, a detailed kinetic and mechanistic study has been performed with NOCbl at pH 7.4 in aqueous solution *(180)*. Only "base-on" NOCbl reacts with O_2, and the reaction proceeds via an associative mechanism involving a Co(III)-$N(O)OO^-$ intermediate, as described above. The latter species undergoes O–O bond homolysis and ligand isomerization to yield NO_2Cbl and H_2OCbl^+/HOCbl, respectively, via the formation of $^{\bullet}OH$ and $^{\bullet}NO_2$ intermediates arising in the homolysis.

The M–(NO^-) and M–(HNO) (M = Fe, Ru) complexes described in this work have been shown to be reactive under an oxygen atmosphere, either in nonaqueous or aqueous media, though no kinetic/mechanistic studies are available *(13–15)*. Once the speciation of the NO^-/HNO complexes is known, there is an obvious need to make advances in the studies on this type of reactivity, particularly in biorelevant aqueous media, with a need of disclosing the similarities and differences with autoxidation reactions of $n = 7$ complexes, like those described in Section 3.4 for $[Fe(CN)_5NO]^{3-}$ and other related nonheme and heme-$\{MX_5NO\}^n$ ions.

5. CONCLUSIONS

The comparative description of structure–reactivity correlations in the $n = 6, 7, 8$ systems (particularly those involving group 8 metal centers holding the same coligand environment) contributed to disclose important

mechanistic features that are interesting in their own right but also in association with biological functions. We have focused on recent advances that deal with several aspects of a diverse (and in some cases well known) scenario. For the $\{M–NO\}^{6,7}$ species, we explore the factors that regulate the stability of 5C/6C complexes, associated with the so-called *trans*-effect and the role of the metal/coligand framework in controlling the electrophilic or nucleophilic reactivities of the MNO moieties. A specific mention to sGC highlights the crucial mechanistic uncertainties still observable in the activation process of this enzyme, and a provocative comment (already raised by others) has been introduced on the possible involvement of dinitrosyls. The role of diverse dinitrosyls appears also as crucial in the chemistry of NO-reductases, though we do have not addressed this issue here.

There have been recent reports on HNO/NO^- coordination chemistry, which have merited a detailed discussion on the structural results, as well as on the chemistry of these species in aqueous solution. For $n=8$, big uncertainties are still detectable on the real speciation, as well as on crucial redox potentials which may control the redox activity of HNO/NO^- in metal-bound systems. Several reports on the pK_a of aqueous bound HNO, though still controversial, suggest that a value of ≈ 10 is a reasonable assignment. However, the experiments still suggest that bound NO^- may be significant to the chemistry even in neutral aqueous solutions, associated with its influence on the release of the *trans*-ligands. Overall, the structure and chemistry of nonheme and heme systems show great resemblance but also specific differences which may be relevant in a biological context.

REFERENCES

1. Enemark, J. H.; Feltham, R. D. *Coord. Chem. Rev.* **1974**, *13*, 339–406.
2. Enemark, J. H.; Feltham, R. D. *Top. Stereochem.* **1981**, *12*, 155–215.
3. (a) Mingos, D. M. P.; Sherman, D. J. *Adv. Inorg. Chem.* **1989**, *34*, 293–377; (b) Richter-Addo, G. B.; Legzdins, P. *Metal Nitrosyls*, Oxford University Press: New York, 1992.
4. Stamler, J. S.; Singel, D. J.; Loscalzo, J. *Science* **1992**, *258*, 1898–1902.
5. (a) Clarke, M. J.; Gaul, J. B. *Struct. Bond.* **1993**, *81*, 147–181; (b) Culotta, E.; Koshland, D. E. *Science* **1992**, *258*, 1862–1865; (c) Westcott, B. L.; Enemark, J. H. *Inorganic Electronic Structure and Spectroscopy*, Vol. II; John Wiley & Sons: New York, 1999; pp 403–450; (d) Moncada, S.; Palmer, R. M. J.; Higgs, E. A. *Pharmacol. Rev.* **1991**, *43*, 109–142; (e) McCleverty, J. A. *Chem. Rev.* **2004**, *104*, 403–418; (f) Feelisch, M.; Stamler, J. S., Eds. *Methods in Nitric Oxide Research*; J. Wiley & Sons: Chichester, 1996; (g) Ignarro, J. L., Ed. *Nitric Oxide, Biology and Pathobiology*; Academic Press: San Diego, 2000; (h) Lancaster, J., Jr., Ed. *Nitric Oxide, Principles and Actions*; Academic Press: San Diego, 1996.
6. Butler, A. R.; Megson, I. L. *Chem. Rev.* **2002**, *102*, 1155–1165.
7. (a) Jorgensen, C. K. *Coord. Chem. Rev.* **1966**, *1*, 164–178; (b) Kaim, W.; Schwerderski, B. *Coord. Chem. Rev.* **2010**, *254*, 1580–1588.

8. Olabe, J. A. *Dalton Trans.* **2008**, 3633–3648.
9. Butler, A. R.; Glidewell, C. *Chem. Soc. Rev.* **1987**, *16*, 361–380.
10. Roncaroli, F.; Olabe, J. A.; van Eldik, R. *Inorg. Chem.* **2003**, *42*, 4179–4189.
11. Roncaroli, F.; van Eldik, R.; Olabe, J. A. *Inorg. Chem.* **2005**, *44*, 2781–2790.
12. González Lebrero, M. C.; Scherlis, D. A.; Estiú, G. L.; Olabe, J. A.; Estrin, D. A. *Inorg. Chem.* **2001**, *40*, 4127–4133.
13. Montenegro, A. C.; Amorebieta, V. T.; Slep, L. D.; Martin, D. F.; Roncaroli, F.; Murgida, D. H.; Bari, S. E.; Olabe, J. A. *Angew. Chem. Int. Ed.* **2009**, *48*, 4213–4216.
14. Montenegro, A. C.; Bari, S. E.; Olabe, J. A. *J. Inorg. Biochem.* **2013**, *118*, 108–114.
15. Osa Codesido, N.; Weyhermüller, T.; Olabe, J. A.; Slep, L. D. *Inorg. Chem.* **2014**, *53*, 981–997.
16. Miranda, K. M. *Coord. Chem. Rev.* **2005**, *249*, 433–455.
17. Farmer, P. J.; Sulc, F. J. *J. Inorg. Biochem.* **2005**, *99*, 166–184.
18. Lehnert, N.; Scheidt, W. R.; Wolf, M. W. *Struct. Bond.* **2014**, *154*, 155–223.
19. Carducci, M. D.; Pressprich, M. R.; Coppens, P. *J. Am. Chem. Soc.* **1997**, *119*, 2669–2678.
20. Pitarch López, J.; Heinemann, F. W.; Prakash, R.; Hess, B. A.; Horner, O.; Jeandey, C.; Oddou, J. L.; Latour, J. M.; Grohmann, A. *Chem. Eur. J.* **2002**, *8*, 5709–5722.
21. Patra, A. K.; Rowland, J. M.; Marlin, D. S.; Bill, E.; Olmstead, M. M.; Mascharak, P. K. *Inorg. Chem.* **2003**, *42*, 6812–6823.
22. Ellison, M. K.; Schulz, C. E.; Scheidt, W. R. *J. Am. Chem. Soc.* **2002**, *124*, 13833–13841.
23. Xu, N.; Goodrich, L. E.; Lehnert, N.; Powell, D. R.; Richter-Addo, G. B. *Angew. Chem. Int. Ed.* **2013**, *52*, 3896–3900.
24. Garcia Serres, R.; Grapperhaus, C. A.; Bothe, E.; Bill, E.; Weyhermuller, T.; Neese, F.; Wieghardt, K. *J. Am. Chem. Soc.* **2004**, *126*, 5138–5153.
25. Xu, N.; Powell, D. R.; Richter-Addo, G. B. *Angew. Chem. Int. Ed.* **2011**, *50*, 9694–9696.
26. Sellmann, D.; Blum, N.; Heinemann, F. W.; Hess, B. A. *Chem. Eur. J.* **2001**, *7*, 1874–1880.
27. Xu, N.; Powell, D. R.; Cheng, L.; Richter-Addo, G. B. *Chem. Commun.* **2006**, 2030–2032.
28. Schweitzer, D.; Ellison, J. J.; Shoner, S. C.; Lovell, S.; Kovacs, J. A. *J. Am. Chem. Soc.* **1998**, *120*, 10996–10997.
29. Richter-Addo, G. B.; Wheeler, R. A.; Hixson, C. A.; Chen, L.; Khan, M. A.; Ellison, M. K.; Schulz, C. E.; Scheidt, W. R. *J. Am. Chem. Soc.* **2001**, *123*, 6314–6326.
30. Videla, M.; Jacinto, J. S.; Baggio, R.; Garland, M. T.; Singh, P.; Kaim, W.; Slep, L. D.; Olabe, J. A. *Inorg. Chem.* **2006**, *45*, 8608–8617.
31. De, P.; Maji, S.; Chowdhury, A. D.; Mobin, S. M.; Mondal, T. K.; Paretzki, A.; Lahiri, G. K. *Dalton Trans.* **2011**, *40*, 12527–12539.
32. Olabe, J. A.; Gentil, L. A.; Rigotti, G. E.; Navaza, A. *Inorg. Chem.* **1984**, *23*, 4297–4302.
33. Bezerra, C. W. B.; da Silva, S. C.; Gambardella, M. T. P.; Santos, R. H. A.; Plicas, L. M. A.; Tfouni, E.; Franco, D. W. *Inorg. Chem.* **1999**, *38*, 5660–5667.
34. Patra, A. K.; Mascharak, P. K. *Inorg. Chem.* **2003**, *42*, 7363–7365.
35. Singh, P.; Das, A. K.; Sarkar, B.; Niemeyer, M.; Roncaroli, F.; Olabe, J. A.; Fiedler, J.; Zalis, S.; Kaim, W. *Inorg. Chem.* **2008**, *47*, 7106–7113.
36. Hadadzadeh, H.; DeRosa, M. C.; Yap, G. P. A.; Rezvani, A. R.; Crutchley, R. J. *Inorg. Chem.* **2002**, *41*, 6521–6526.
37. Bottomley, F. *J. Chem. Soc. Dalton Trans.* **1974**, 1600–1605.

38. Osa Codesido, N.; De Candia, A. G.; Weyhermuller, T.; Olabe, J. A.; Slep, L. D. *Eur. J. Inorg. Chem.* **2012**, 4301–4309.
39. Scheidt, W. R.; Lee, Y. J.; Hatano, K. *J. Am. Chem. Soc.* **1984**, *106*, 3191–3198.
40. Xu, N.; Lilly, J.; Powell, D. R.; Richter-Addo, G. B. *Organometallics* **2012**, *31*, 827–834.
41. Baraldo, L. M.; Bessega, M. S.; Rigotti, G. E.; Olabe, J. A. *Inorg. Chem.* **1994**, *33*, 5890–5896.
42. Carter, S. M.; Lee, J.; Hixson, C. A.; Powell, D. R.; Wheeler, R. A.; Shaw, M. J.; Richter-Addo, G. B. *Dalton Trans.* **2006**, 1338–1346.
43. Linder, D. P.; Rodgers, K. R.; Banister, J.; Wyllie, G. R. A.; Ellison, M. K.; Scheidt, W. R. *J. Am. Chem. Soc.* **2004**, *126*, 14136–14148.
44. Lee, C. M.; Chen, C. H.; Chen, H. W.; Hsu, J. L.; Lee, G. H.; Liaw, W. F. *Inorg. Chem.* **2005**, *44*, 6670–6679.
45. Goodrich, L. E.; Paulat, F.; Praneeth, V. K. K.; Lehnert, N. *Inorg. Chem.* **2010**, *49*, 6293–6316.
46. Averill, B. A. *Chem. Rev.* **1996**, *96*, 2951–2964.
47. Wasser, I. M.; de Vries, S.; Moenne-Loccoz, P.; Schroder, I.; Karlin, K. D. *Chem. Rev.* **2002**, *102*, 1201–1234.
48. Endo, I.; Odaka, M.; Yohada, M. *Trends Biotechnol.* **1999**, *17*, 244–248.
49. (a) Butler, A. R.; Glidewell, C.; Li, M. H. *Adv. Inorg. Chem.* **1988**, *32*, 335–393; (b) Lewandowska, H. *Struct. Bond.* **2014**, *153*, 45–114.
50. Ford, P. C.; Bourassa, J.; Miranda, K.; Lee, B.; Lorkovic, I.; Boggs, S.; Kudo, S.; Laverman, L. *Coord. Chem. Rev.* **1998**, *171*, 185–202.
51. (a) Artaud, I.; Chatel, S.; Chauvin, A. S.; Bonnet, D.; Kopf, M. A.; Leduc, P. *Coord. Chem. Rev.* **1999**, *190–192*, 577–586; (b) Harrop, T. C.; Mascharak, P. K. *Acc. Chem. Res.* **2004**, *37*, 253–260.
52. Fry, N. L.; Mascharak, P. K. *Dalton Trans.* **2012**, *41*, 4726–4735.
53. (a) Scheidt, W. R.; Ellison, M. K. *Acc. Chem. Res.* **1999**, *32*, 350–359; (b) Cheng, L.; Richter-Addo, G. B. In: *The Porphyrin Handbook*; Kadish, K. M.; Smith, K. M.; Guillard, R. Eds.; Academic Press: New York, 2000, pp 219–291; (c) Wyllie, G. R. A.; Scheidt, W. R. *Chem. Rev.* **2002**, *102*, 1067–1089.
54. (a) Shimizu, H.; Obayashi, E.; Gomi, Y.; Arakawat, S.; Park, Y.; Nakamura, S.; Adachi, I.; Shoun, H.; Shiro, Y. *J. Biol. Chem.* **2000**, *275*, 4816–4826; (b) Pant, K.; Crane, B. R. *Biochemistry* **2006**, *45*, 2537–2544.
55. Paulat, F.; Lehnert, N. *Inorg. Chem.* **2007**, *46*, 1547–1549.
56. Toledo, J. C.; dos Santos Lima Neto, B.; Franco, D. W. *Coord. Chem. Rev.* **2005**, *249*, 419–431.
57. Patra, A. K.; Rose, M. J.; Olmstead, M. M.; Mascharak, P. K. *J. Am. Chem. Soc.* **2004**, *126*, 4780–4781.
58. Sellmann, D.; Utz, J.; Heinemann, F. W. *Inorg. Chem.* **1999**, *38*, 5314–5322.
59. (a) Fomitchev, D. V. V.; Coppens, P. *Inorg. Chem.* **1996**, *35*, 7021–7026; (b) Togano, T.; Kuroda, H.; Nagao, N.; Maekawa, Y.; Nishimura, H.; Howell, F. S.; Mukaida, M. *Inorg. Chim. Acta* **1992**, *196*, 57–63.
60. Veal, T. J.; Hodgson, D. J. *Inorg. Chem.* **1972**, *11*, 1420–1424.
61. Wolak, M.; van Eldik, R. *J. Am. Chem. Soc.* **2005**, *127*, 13312–13315.
62. Merkle, A. C.; Fry, N. L.; Mascharak, P. K.; Lehnert, N. *Inorg. Chem.* **2011**, *50*, 12192–12203.
63. Eroy-Reveles, A. A.; Leung, Y.; Beavers, C. M.; Olmstead, M. M.; Mascharak, P. K. *J. Am. Chem. Soc.* **2008**, *130*, 4447–4458.
64. Franz, K. J.; Lippard, S. J. *J. Am. Chem. Soc.* **1998**, *120*, 9034–9040.
65. Manoharan, P. T.; Gray, H. B. *Inorg. Chem.* **1966**, *6*, 823–839.
66. Hummel, P.; Winkler, J. R.; Gray, H. B. *Theor. Chem. Acc.* **2008**, *119*, 35–38.

67. Manoharan, P. T.; Gray, H. B. *J. Am. Chem. Soc.* **1965**, *87*, 3340–3348.
68. Gorelsky, S. I.; da Silva, S. C.; Lever, A. B. P.; Franco, D. W. *Inorg. Chim. Acta* **2000**, *300*, 698–708.
69. Praneeth, V. K. K.; Paulat, F.; Berto, T. C.; DeBeer George, S.; Nather, C.; Sulok, C. D.; Lehnert, N. *J. Am. Chem. Soc.* **2008**, *130*, 15288–15303.
70. Olabe, J. A. In: *Physical Inorganic Chemistry, Processes and Applications*; Bakac, A. Ed.; Wiley: Hoboken, 2010 pp 281–337.
71. (a) Olabe, J. A.; Slep, L. D. In: Mc Cleverty, J. A., Meyer, T. J., Eds.; Comprehensive Coordination Chemistry II, from Biology to Nanotechnology, Vol. 1; Elsevier: Oxford, 2004; pp 603–623; (b) Roncaroli, F.; Videla, M.; Slep, L. D.; Olabe, J. A. *Coord. Chem. Rev.* **2007**, *251*, 1903–1930.
72. (a) Franke, A.; Roncaroli, F.; van Eldik, R. *Eur. J. Inorg. Chem.* **2007**, 773–798; (b) Tfouni, E.; Krieger, M.; McGarvey, B. R.; Franco, D. W. *Coord. Chem. Rev.* **2003**, *236*, 57–69; (c) Wanat, A.; Wolak, M.; Orzel, L.; Brindell, M.; van Eldik, R.; Stochel, G. *Coord. Chem. Rev.* **2002**, *229*, 37–49; (d) Wolak, M.; van Eldik, R. *Coord. Chem. Rev.* **2002**, *230*, 263–282.
73. (a) Lim, M. D.; Lorkovic, I. M.; Ford, P. C. *J. Inorg. Biochem.* **2005**, *99*, 151–165; (b) Ford, P. C.; Fernandez, B. O.; Lim, M. D. *Chem. Rev.* **2005**, *105*, 2439–2455; (c) Ford, P. C.; Laverman, L. E.; Lorkovic, I. *Adv. Inorg. Chem.* **2003**, *54*, 203–257; (d) Ford, P. C.; Melo Pereyra, J. C.; Miranda, K. M. *Struct. Bond.* **2014**, *154*, 99–135.
74. Ford, P. C.; Laverman, L. E. *Coord. Chem. Rev.* **2005**, *249*, 391–403.
75. Baraldo, L. M.; Forlano, P.; Parise, A. R.; Slep, L. D.; Olabe, J. A. *Coord. Chem. Rev.* **2001**, *219*, 881–921.
76. Roncaroli, F.; Olabe, J. A.; van Eldik, R. *Inorg. Chem.* **2002**, *41*, 5417–5425.
77. Rosokha, S. V.; Kochi, J. K. *J. Am. Chem. Soc.* **2001**, *123*, 8985–8999.
78. Odaka, M.; Fujii, K.; Hoshino, M.; Noguchi, T.; Tsujimura, M.; Nagashima, S.; Yohda, M.; Nagamune, T.; Inoue, Y.; Endo, I. *J. Am. Chem. Soc.* **1997**, *119*, 3785–3791.
79. Oszajca, M.; Franke, A.; Brindell, M.; Stochel, G.; van Eldik, R. *Inorg. Chem.* **2011**, *50*, 3413–3424.
80. Toma, H. E.; Malin, J. M. *J. Am. Chem. Soc.* **1975**, *97*, 288–293.
81. Toma, H. E.; Malin, J. M. *Inorg. Chem.* **1973**, *12*, 1039–1045.
82. Toma, H. E.; Batista, A. A.; Gray, H. B. *J. Am. Chem. Soc.* **1982**, *104*, 7509–7515.
83. Ilkowska, E.; Lewinski, K.; van Eldik, R.; Stochel, G. *J. Biol. Inorg. Chem.* **1999**, *4*, 302–310.
84. Czap, A.; van Eldik, R. *Dalton Trans.* **2003**, 665–671.
85. (a) Zanichelli, P. G.; Miotto, A. M.; Estrela, H. F. G.; Rocha Soares, F.; Grassi-Kassisse, D. N.; Spadari-Bratfisch, R. C.; Castellano, R. C.; Roncaroli, F.; Parise, A. R.; Olabe, J. A.; de Brito, R. M. S.; Franco, D. W. *J. Inorg. Biochem.* **2004**, *98*, 1921–1932; (b) Cameron, B. R.; Darkes, M. C.; Yee, H.; Olsen, M.; Fricker, S. P.; Skerlj, R. T.; Bridger, G. J.; Davies, N. A.; Wilson, M. T.; Rose, D. J.; Zubieta, J. *Inorg. Chem.* **2003**, *42*, 1868–1876.
86. Matsubara, T.; Creutz, C. *Inorg. Chem.* **1979**, *18*, 1957–1966.
87. Czap, A.; Heinemann, F. W.; van Eldik, R. *Inorg. Chem.* **2004**, *43*, 7832–7843.
88. Videla, M.; Braslavsky, S. E.; Olabe, J. A. *Photochem. Photobiol. Sci.* **2005**, *4*, 75–82.
89. Olabe, J. A.; Estiu, G. L. *Inorg. Chem.* **2003**, *42*, 4873–4880.
90. Bottomley, F. In Reactions of Coordinated Ligands; Vol. 2; Plenum Publisher Corp: New York, 1989.
91. Olabe, J. A. *Adv. Inorg. Chem.* **2004**, *55*, 61–126.
92. Roncaroli, F.; Ruggiero, M. E.; Franco, D. W.; Estiu, G. L.; Olabe, J. A. *Inorg. Chem.* **2002**, *41*, 5760–5769.
93. Gutierrez, M. M.; Amorebieta, V. T.; Estiú, G. L.; Olabe, J. A. *J. Am. Chem. Soc.* **2002**, *124*, 10307–10319.

94. (a) Gutierrez, M. M.; Alluisetti, G. B.; Olabe, J. A.; Amorebieta, V. T. *Dalton Trans.* **2008**, 5025–5030; (b) Gutierrez, M. M.; Olabe, J. A.; Amorebieta, V. T. *Eur. J. Inorg. Chem.* **2012**, 4433–4438.
95. Wolfe, S. K.; Andrade, C.; Swinehart, J. H. *Inorg. Chem.* **1974**, *13*, 2567–2572.
96. (a) Schwane, J. D.; Ashby, M. T. *J. Am. Chem. Soc.* **2002**, *124*, 6822–6823; (b) Szacilowski, K.; Stochel, G.; Stasicka, Z.; Kisch, H. *New J. Chem.* **1997**, *21*, 893–902.
97. (a) Szacilowski, K.; Wanat, A.; Barbieri, A.; Wasiliewska, E.; Witko, M.; Stochel, G.; Stasicka, Z. *New J. Chem.* **2002**, *26*, 1495–1502; (b) Morando, P. J.; Borghi, E. B.; Schteingart, L. M.; Blesa, M. A. *J. Chem. Soc. Dalton Trans.* **1981**, 435–440.
98. Roncaroli, F.; Olabe, J. A. *Inorg. Chem.* **2005**, *14*, 4719–4727.
99. Quiroga, S. L.; Almaraz, A. E.; Amorebieta, V. T.; Perisinotti, L. L.; Olabe, J. A. *Chem. Eur. J.* **2011**, *17*, 4145–4156.
100. Filipovic, M. R.; Eberhardt, M.; Prokopovic, V.; Mijuskovic, A.; Orescanin-Dusic, Z.; Reeh, P.; Ivanovic-Burmazovic, I. *J. Med. Chem.* **2013**, *56*, 1499–1508.
101. (a) Whiteman, M.; Moore, P. K. *J. Cell. Mol. Med.* **2009**, *13*, 488–507; (b) Li, L.; Rose, P.; Moore, P. K. *Annu. Rev. Pharmacol. Toxicol.* **2011**, *51*, 1169–1187.
102. Fernandez, B. O.; Lorkovic, I. M.; Ford, P. C. *Inorg. Chem.* **2004**, *43*, 5393–5402.
103. (a) Hoshino, M.; Laverman, L.; Ford, P. C. *Coord. Chem. Rev.* **1999**, *187*, 75–102; (b) Ford, P. C.; Lorkovic, I. M. *Chem. Rev.* **2002**, *102*, 993–1018.
104. Jee, J. E.; Eigler, S.; Jux, N.; Zahl, A.; van Eldik, R. *Inorg. Chem.* **2007**, *46*, 3336–3352.
105. Li, J.; Banerjee, A.; Pawlak, P. L.; Brennessel, W. W.; Chavez, F. A. *Inorg. Chem.* **2014**, *53*, 5414–5416.
106. Park, H.; Bittner, M. M.; Baus, J. S.; Lindeman, S. V.; Fiedler, A. T. *Inorg. Chem.* **2012**, *51*, 10279–10289.
107. Berto, T. C.; Hoffman, M. B.; Murata, Y.; Landenberger, K. B.; Alp, E. E.; Zhao, J.; Lehnert, N. *J. Am. Chem. Soc.* **2011**, *133*, 16714–16717.
108. Pohl, K.; Wieghardt, K.; Nuber, B.; Weiss, J. *J. Chem. Soc. Dalton Trans.* **1987**, 187–192.
109. McQuilken, A. C.; Ha, Y.; Sutherlin, K. D.; Siegler, M. A.; Hodgson, K. O.; Hedman, B.; Solomon, E. I.; Jameson, G. N. L.; Goldberg, D. P. *J. Am. Chem. Soc.* **2013**, *135*, 14024–14027.
110. Wyllie, G. R. A.; Schultz, F. A.; Scheidt, W. R. *Inorg. Chem.* **2003**, *42*, 5722–5734.
111. Hauser, C.; Glaser, T.; Bill, E.; Weyhermuller, T.; Wieghardt, K. *J. Am. Chem. Soc.* **2000**, *122*, 4352–4365.
112. Nast, R.; Schmidt, J. *Z. Anorg. Allg. Chem.* **1976**, *421*, 15–23.
113. Hodges, K. D.; Wollmann, R. G.; Kessel, S. L.; Hendrickson, D. N.; Vanderveer, D. G.; Barefield, E. K. *J. Am. Chem. Soc.* **1979**, *101*, 906–917.
114. Ray, M.; Golombek, A. P.; Hendrich, M. P.; Yap, G. P. A.; Liable-Sands, L. M.; Rheingold, A. L.; Borovik, A. S. *Inorg. Chem.* **1999**, *38*, 3110–3115.
115. (a) Speelman, A. L.; Lehnert, N. *Angew. Chem. Int. Ed.* **2013**, *52*, 12283–12287; (b) Speelman, A. L.; Lehnert, N. *Acc. Chem. Res.* **2014**, *47*, 1106–1116.
116. Goodrich, L. E.; Roy, S.; Alp, E. E.; Zhao, J.; Hu, M. Y.; Lehnert, N. *Inorg. Chem.* **2013**, *52*, 7766–7780.
117. Schmidt, J.; Kühr, H.; Dorn, W. L.; Kopf, J. *Inorg. Nucl. Chem. Lett.* **1974**, *10*, 55–61.
118. Franz, K. J.; Lippard, S. J. *J. Am. Chem. Soc.* **1999**, *121*, 10504–10512.
119. Maxwell, J. C.; Caughey, W. S. *Biochemistry* **1976**, *121*, 10504–10512.
120. Silvernail, N. J.; Olmstead, M. M.; Noll, B. C.; Scheidt, W. R. *Inorg. Chem.* **2009**, *48*, 971–977.
121. Harrop, T. C.; Olmstead, M. M.; Mascharak, P. K. *Inorg. Chem.* **2005**, *44*, 6918–6920.
122. Wanner, M.; Scheiring, T.; Kaim, W.; Slep, L. D.; Baraldo, L. M.; Olabe, J. A.; Zalis, S.; Baerends, E. J. *Inorg. Chem.* **2001**, *40*, 5704–5707.
123. (a) van Voorst, J. D. W.; Hemmerich, P. J. *J. Chem. Phys.* **1966**, *45*, 3914; (b) Glidewell, C.; Johnson, I. L. *Inorg. Chim. Acta* **1987**, *132*, 145–147.

124. (a) Frantz, S.; Sarkar, B.; Sieger, M.; Kaim, W.; Roncaroli, F.; Olabe, J. A.; Zalis, S. *Eur. J. Inorg. Chem.* **2004**, 2902–2907; (b) McGarvey, B. R.; Ferro, A. A.; Tfouni, E.; Bezerra, C. W. B.; Bagatin, I.; Franco, D. W. *Inorg. Chem.* **2000**, *39*, 3577–3581.
125. Praneeth, V. K. K.; Neese, F.; Lehnert, N. *Inorg. Chem.* **2005**, *44*, 2570–2572.
126. Praneeth, V. K. K.; Nather, C.; Peters, G.; Lehnert, N. *Inorg. Chem.* **2006**, *45*, 2795–2811.
127. Lehnert, N.; Sage, J. T.; Silvernail, N.; Scheidt, W. R.; Alp, E. E.; Sturhahn, W.; Zhao, J. *Inorg. Chem.* **2010**, *49*, 7197–7215.
128. Brown, C. A.; Pavlovsky, M. A.; Westre, T. E.; Zhang, Y.; Hedman, B.; Hodgson, K. O.; Solomon, E. I. *J. Am. Chem. Soc.* **1995**, *17*, 715–732.
129. Wanat, A.; Schneppensieper, T.; Stochel, G.; van Eldik, R.; Bill, E.; Wieghardt, K. *Inorg. Chem.* **2002**, *41*, 4–10.
130. Arciero, D. M.; Lipscomb, J. D.; Huynh, B. H.; Kent, T. A.; Munck, E. J. *J. Biol. Chem.* **1983**, *258*, 4981–4991.
131. (a) Schneppensieper, T.; Finkler, S.; Czap, A.; van Eldik, R.; Heus, M.; Nieuwenhuizen, P.; Wreesmann, C.; Abma, W. *Eur. J. Inorg. Chem.* **2001**, 491–501; (b) Schneppensieper, T.; Wanat, A.; Stochel, G.; Goldstein, S.; Meyerstein, D.; van Eldik, R. *Eur. J. Inorg. Chem.* **2001**, 2317–2325; (c) Schneppensieper, T.; Wanat, A.; Stochel, G.; van Eldik, R. *Inorg. Chem.* **2002**, *41*, 2565–2573.
132. Hammes, B. S.; Ramos-Maldonado, D.; Yap, G. P. A.; Liable-Sands, L.; Rheingold, A. L.; Young, V. G., Jr.; Borovik, A. S. *Inorg. Chem.* **1997**, *36*, 3210–3211.
133. Traylor, T. G.; Sharma, V. S. *Biochemistry* **1992**, *31*, 2847–2849.
134. Cheney, R. P.; Simic, M. G.; Hoffman, M. Z.; Taub, I. A.; Asmus, K. D. *Inorg. Chem.* **1997**, *16*, 2187–2192.
135. Cheney, R. P.; Hoffman, M. Z.; Lust, J. A. *Inorg. Chem.* **1978**, *17*, 1177–1180.
136. (a) Berto, T. C.; Speelman, A. L.; Zheng, S.; Lehnert, N. *Coord. Chem. Rev.* **2013**, *257*, 244–259; (b) Xu, N.; Yi, J.; Richter-Addo, G. B. *Inorg. Chem.* **2010**, *49*, 6253–6266.
137. (a) Wilcox, D. E.; Kruszina, D. E.; Smith, R. P. *Chem. Res. Toxicol.* **1990**, *3*, 71–76; (b) Bates, J. N.; Baker, M. T.; Guerra, R., Jr.; Harrison, D. G. *Biochem. Pharmacol.* **1991**, *42*, S157–S165.
138. Zerga, H. O.; Olabe, J. A. *Inorg. Chem.* **1983**, *22*, 4156–4158.
139. (a) Lorkovic, I.; Ford, P. C. *J. Am. Chem. Soc.* **2000**, *122*, 6516–6517; (b) Patterson, J. C.; Lorkovic, I.; Ford, P. C. *Inorg. Chem.* **2003**, *42*, 4902–4908; (c) Conradie, J.; Wondimagegn, T.; Ghosh, A. *J. Am. Chem. Soc.* **2003**, *125*, 4968–4969.
140. (a) Foster, M. W.; Cowan, J. A. *J. Am. Chem. Soc.* **1999**, *121*, 4093–4100; (b) Vanin, A. F.; Stukan, R. A.; Mabuchkina, E. B. *Biochim. Biophys. Acta* **1996**, *1295*, 5–12; (c) EUeno, T.; Suzuki, Y.; Fujii, S.; Vanin, A. F. *Biochem. Pharmacol.* **2002**, *63*, 485–493; (d) Burlamacchi, L.; Martin, G.; Tiezzi, E. *Inorg. Chem.* **1969**, *8*, 2021–2025.
141. Derbyshire, E. R.; Marletta, M. A. *Annu. Rev. Biochem.* **2012**, *81*, 533–559.
142. Ballou, D. P.; Zhao, Y.; Brandish, P. E.; Marletta, M. A. *Proc. Natl. Acad. Sci. USA* **2002**, *99*, 12097–12101.
143. Zhao, Y.; Brandish, P. E.; Ballou, D. P.; Marletta, M. A. *Proc. Natl. Acad. Sci. USA* **1999**, *96*, 14753–14758.
144. Martí, M. A.; Capece, L.; Crespo, A.; Doctorovich, F.; Estrin, D. A. *J. Am. Chem. Soc.* **2005**, *127*, 7721–7728.
145. Moller, J. K. S.; Skibsted, L. H. *Chem. Eur. J.* **2004**, *10*, 2291–2300.
146. Videla, M.; Roncaroli, F.; Slep, L. D.; Olabe, J. A. *J. Am. Chem. Soc.* **2007**, *129*, 278–279.
147. Armor, J. N.; Hoffman, M. Z. *Inorg. Chem.* **1975**, *14*, 444–446.

148. Cheng, L.; Powell, D. R.; Khan, M. A.; Richter-Addo, G. B. *Chem. Commun.* **2000**, 2301–2302.
149. Callahan, R. W.; Meyer, T. J. *Inorg. Chem.* **1977**, *16*, 574–581.
150. Snyder, D. A.; Weaver, D. L. *Inorg. Chem.* **1970**, *9*, 2760–2767.
151. Hannibal, L.; Smith, C. A.; Jacobsen, D. W.; Brasch, N. E. *Angew. Chem. Int. Ed.* **2007**, *46*, 5140–5143.
152. Grande, L. M.; Noll, B. C.; Oliver, A. G.; Scheidt, W. R. *Inorg. Chem.* **2010**, *49*, 6552–6557.
153. Franz, K. J.; Doerrer, L. H.; Spingler, B.; Lippard, S. J. *Inorg. Chem.* **2001**, *40*, 3774–3780.
154. Sanders, B. C.; Patra, A. K.; Harrop, T. C. *J. Inorg. Biochem.* **2013**, *118*, 115–127.
155. Pellegrino, J.; Bari, S. E.; Bikiel, D. E.; Doctorovich, F. *J. Am. Chem. Soc.* **2010**, *132*, 989–995.
156. Immoos, C. E.; Sulc, F. J.; Farmer, P. J.; Czarnecki, K.; Bocian, D.; Levina, A.; Aitken, J. B.; Armstrong, R.; Lay, P. A. *J. Am. Chem. Soc.* **2005**, *127*, 814–815.
157. Sellmann, D.; Gottschalk-Gaudig, T.; Haussinger, D.; Heinemann, F. W.; Hess, B. A. *Chem. Eur. J.* **2001**, *7*, 2099–2103.
158. Wilson, R. D.; Ibers, J. A. *Inorg. Chem.* **1979**, *18*, 336–343.
159. Melenkivitz, R.; Hillhouse, G. L. *Chem. Commun.* **2002**, *2*, 660–661.
160. Scheidt, W. R.; Hoard, J. L. *J. Am. Chem. Soc.* **1973**, *95*, 8281–8288.
161. Patra, A. K.; Dube, K. S.; Sanders, B. C.; Papaefthymiou, G. C.; Conradie, J.; Ghosh, A.; Harrop, T. C. *Chem. Sci.* **2012**, *3*, 364–369.
162. Lehnert, N.; Praneeth, V. K. K.; Paulat, F. *J. Comput. Chem.* **2006**, *27*, 1338–1351.
163. Hassanin, H. A.; Hannibal, L.; Jacobsen, D. W.; Brown, K. L.; Marques, H. M.; Brasch, N. E. *Dalton Trans.* **2009**, 424–433.
164. Suarez, S. A.; Fonticelli, M. H.; Rubert, A. A.; de la LLave, E.; Scherlis, D. A.; Salvarezza, R. C.; Martí, M. A.; Doctorovich, F. *Inorg. Chem.* **2010**, *49*, 6955–6966.
165. (a) Kelly, B. A.; Welch, A. J.; Woodward, P. *J. Chem. Soc. Dalton Trans.* **1977**, 2237–2242; (b) Schaniel, D.; Woike, T.; Behrnd, N.-R.; Hauser, J.; Krämer, K. W.; Todorova, T.; Delley, B. *Inorg. Chem.* **2009**, *48*, 11399–11406.
166. Roper, W. R.; Grundy, K. R.; Reed, C. R. *J. Chem. Soc. Chem. Commun.* **1970**, *22*, 1501–1502.
167. Doctorovich, F.; Bikiel, D. E.; Pellegrino, J.; Suárez, S. A.; Martí, M. A. *Adv. Inorg. Chem.* **2012**, *64*, 97–139.
168. Southern, J. S.; Hillhouse, G. L.; Rheingold, A. L. *J. Am. Chem. Soc.* **1997**, *119*, 12406–12407.
169. Kumar, M. R.; Fukuto, J. M.; Miranda, K. M.; Farmer, P. J. *Inorg. Chem.* **2010**, *49*, 6283–6292.
170. Yang, L.; Fang, W.; Zhang, Y. *Chem. Commun.* **2012**, *48*, 3842–3844.
171. Dierks, E. A.; Hu, S.; Vogel, K. M.; Yu, A. E.; Spiro, T. G.; Burstyn, J. N. *J. Am. Chem. Soc.* **1997**, *119*, 7316–7323.
172. Goodrich, L. E.; Lehnert, N. *J. Inorg. Biochem.* **2013**, *118*, 179–186.
173. Shafirovich, V.; Lymar, S. V. *Proc. Natl. Acad. Sci. USA* **2002**, *99*, 7340–7345.
174. Masek, J.; Maslova, E. *Collect. Czechoslov. Chem. Commun.* **1974**, *39*, 2141–2161.
175. Gao, Y.; Toubaei, A.; Kong, X.; Wiu, G. *Angew. Chem. Int. Ed.* **2014**, *53* (43), 11547–11551.
176. Lang, D. R.; Davis, J. A.; Lopes, L. G. F.; Ferro, A. A.; Vasconcellos, L. C. G.; Franco, D. W.; Tfouni, E.; Wieraszko, A.; Clarke, M. J. *Inorg. Chem.* **2000**, *39*, 2294–2300.
177. Marti, M. A.; Bari, S. E.; Estrin, D. A.; Doctorovich, F. *J. Am. Chem. Soc.* **2005**, *127*, 4680–4684.

178. Clarkson, S. G.; Basolo, F. *Inorg. Chem.* **1973**, *12*, 1528–1534.
179. (a) Trogler, W. C.; Marzilli, L. G. *Inorg. Chem.* **1974**, *13*, 1008–1010; (b) Grundy, K. R.; Laing, K. R.; Roper, W. R. *J. Chem. Soc. Chem. Commun.* **1970**, 1500–1501; (c) Kubota, M.; Phillips, D. A. *J. Am. Chem. Soc.* **1975**, *16*, 5637–5638.
180. Subedi, H.; Brasch, N. E. *Inorg. Chem.* **2013**, *52*, 11608–11617.